University of Padua

Technical University of Graz

A thesis presented for the degree of Master of Electrical Engineering

Genetic Algorithm Optimization of a Synchronous Reluctance Motor

Student

Eduardo Bonato

Supervisors

Res. Javier M.G.Tenorio

Prof. Klaus Krischan

Prof. Annette Mütze

Prof. Nicola Bianchi

Academic year 2014/2015

Contents

Abstract

This thesis was done in the Institute of Electric Drives and Machines, Technical University of Graz. The project is focused on the design of Synchronous Reluctance Motors and the study about this motor can be used for household applications. The target of the motor is to achieve high efficiency and low cost. At the moment, single phase induction motors are the most common units for home appliances. The reason for this choice is its low production cost. Synchronous reluctance motor, operated as a variable speed drive, can be more qualified candidates for this type of application. The design is carried out by a simple mathematical model and the analysis is used the finite element software COMSOL. For this reason, the aim of the thesis is to create a motor with high efficiency and lower cost in an operating point that is 10 times less the value of its rated power. The motor is optimized with a Genetic Algorithm, which allows to choose the best candidates to achieve the target.

Acknowledgements

I would like to express my heartfelt appreciation to my supervisor, Res. Javier M. G. Tenorio, for his support and continuous help. His knowledge, guidance, understanding and patience inspired the completion of this thesis. I am very grateful to work with such an insightful and caring person. My sincere gratitude also goes to the Professors Klaus Krischan, Annette Mütze and Nicola Bianchi for their valuable advice and help during the months that I spent at the Technical University of Graz. I would like also to acknowledge all the staff of the Institute of Electric Drives and Machines for their help and kindness during these months. I would like to acknowledge the Department of Electrical Engineering at the Padua University for providing an excellent academic environment. I would like to extend my sincere appreciation to my fellow colleagues and friends of all these years at the University of Padova: Dr. Francesco Peretti, Dr. Francesco Rui, Dr. Matteo Mattiazzo, Dr. Francesco Gentilin, Dr. Michele Pepe, Dr. Claudio Zanarello, Dr. Alessandro Zaghetto, Dr. Lucia Mariani, Dr. Francesco Dugatto and Mauro Scarparo. Also, for all the friends which I met during my Erasmus stay in Graz: Irfan Šehić, Jasmin Mustafic, Szecsó Szendródy, Muhamed Redžić, Patick Salman and Anna Slanov. I am flattered for their friendship and for so many good memories throughout my time at Technical University of Graz.

Last but not the least; I would like to thank my parents, my sisters and my beloved Giada, for their patience, care and endless devotion. I am very grateful to my dad that teached me to be strong. Also, I am deeply indebted to my mom for her patience and her prayers. I believe without them I would have been lost.

Chapter 1

Introduction

The aim of the project is to study the optimization of a Synchronous Reluctance Motor for refrigerators household applications. The requirements are design the motor for two different operating points: the rated power point is equal to 100W and at an operating point of 10W the motor should have an efficiency of 95%. One important constraint of this motor is the fact that the windings should be concentrated. This choice is due to the low ohmic resistance motivated by short end-windings and low manufacturing costs.

1.1 Thesis motivation

Electric motors are used extensively in households and industries applications. In Europe, they represent the 40% of the global consume. The most employed units are single phase induction motors where the efficiency is around 70-80%. The efficiency level can be improved using permanent magnet motors, which allow variable speed drives. Due to the high cost of magnets, brushless motors are not an economic alternative. For this reason, synchronous reluctance motors can be an interesting solution, since they do not have magnets. The main characteristics of these motors are the low construction price and be a "cold rotor".

Chapter 2

Mathematical model

A mathematical model represents a description of a physical system. It helps to explain singular effects interacting between them. The complexity of the rotor shape is linked to the anisotropy of the motor, and as a consequence the torque. A common disadvantage of these machines is the high value of torque ripple [1]. That is due to the interaction between the stator MMF spatial harmonics and the permeance harmonics, high iron losses and noise caused by the vibration.

Fig.2.1 shows an example of the shape of the rotor with two flux barriers and different angular openings. The reluctance machine with transversely laminated rotor is a good competitor in fact of high dynamic, high torque density and fault-tolerant capability than other types of electric motors [2]. To increase the power factor of this type of machine, which is usually low, the permanent magnets are inserted. This configuration is called PM-assisted synchronous reluctance machine, Fig.2.2. The goal of the permanent magnet is to increase the saturation of the magnetic ribs.

It is possible to obtain a reasonable reduction of the torque ripple with a suitable choice of the number of flux barriers and the number of the stator slots. Another method consist in shifting the flux barriers from their symmetrical position.

This chapter studies the link between the expression of the torque and the shape of the motor. The rotor geometry has an important influence on the performance of the machine, as shown in [3]. The analytical model, that is a function of the geometry of the motor, allows to compute both the air gap radial flux-density and the electromagnetic motor torque. The analytical model shows the effect of the flux-barriers.

The geometrical variables are angle of the flux-barrier ends θ_b, lenght of the flux-barriers l_b, thickness of the flux-barriers t_b, bore diameter D, stack length L_{stk}, number of slots Q_s and rotor position θ_m, represented in Fig.2.3.

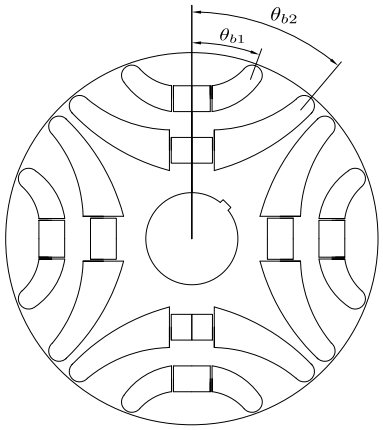

Figure 2.1: Shape of the rotor in a synchronous reluctance machine having two flux barriers

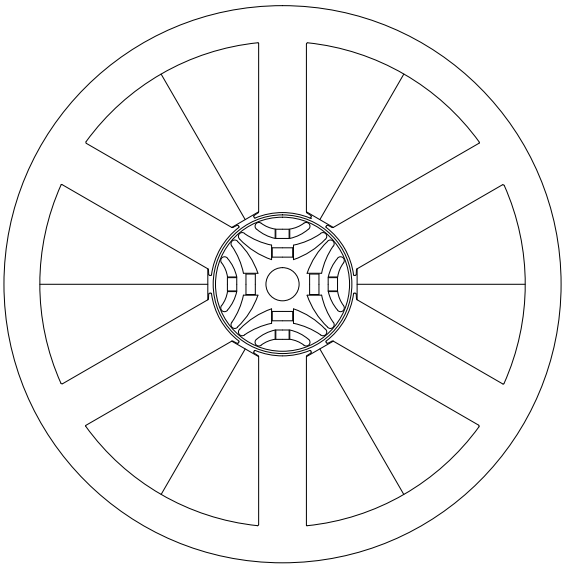

Figure 2.2: PM-assisted syncrhonous reluctance motor

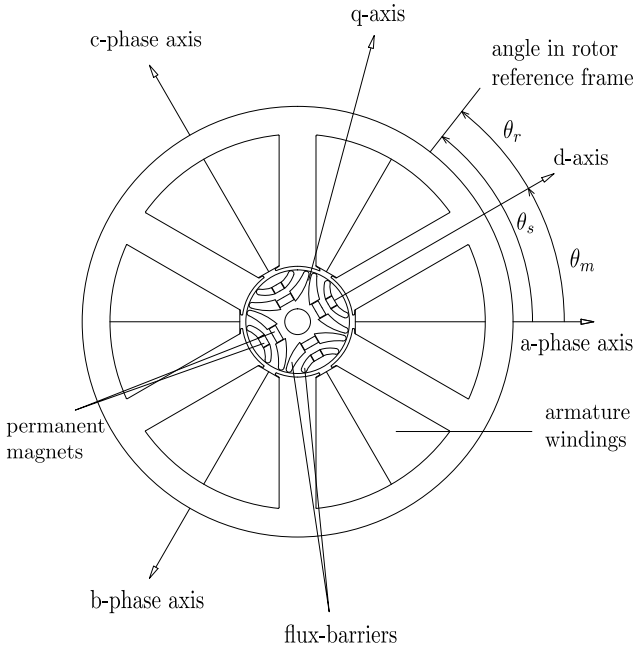

Figure 2.3: Reference of the synchronous reluctance machine

2.1 Magnetic design

Starting from the model, only the reluctance effect is considered (avoiding the permanents magnets). The d-axis is aligned with the rotor path that exhibits a high permeance. The q-phase axis is shifted $\pi/2$ electrical radians. The a-phase coincides with the stator reference axis, while phase b and c are shifted $2\pi/3$ and $4\pi/3$ respectively. This model is linear [4], i.e. it avoids the saturation effects (only for the magnetic ribs) and the iron permeability is considered infinite.

To take care of the magnetic drop in the iron it is necessary increase the actual airgap g_{act}, to consider the assumption of the infinite iron permeability.

$$g = k_{Carter} k_{sat} g_{act} \tag{2.1}$$

where the saturation factor k_{sat}, is the ratio between the total magnetic drop and the magnetic drop in the actual airgap g_{act} and the carter factor k_{Carter} is a coefficient that increase the airgap in case slot opening are considered. The synchronous reluctance motor has its winding placed around the geometry of the stator in order to obtain a sinusoidal magnetic field, that rotates in the air gap. The distribution of conductors phase a can be written as follows

$$n_{da}(\theta) = \hat{n}_d \sin(p\theta_s) \tag{2.2}$$

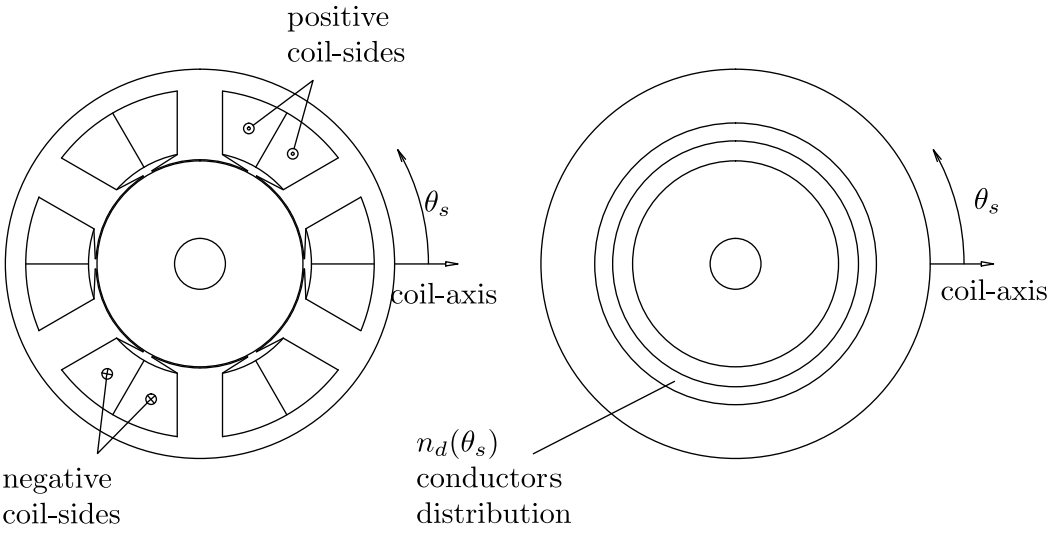

Figure 2.4: Conductors slot distribution

where θ_s is the mechanical angular position in the reference frame of the stator and $\hat{n}_d$ is defined as

$$\hat{n}_d = \frac{4}{\pi}\frac{k_w N}{2D} \tag{2.3}$$

Where D is the bore diameter and k_w is the winding factor obtained by the product of the distribution factor k_d, the pitch factor k_p and the skew factor k_{sk}.

$$k_w = k_d k_p k_{sk} \tag{2.4}$$

with this assumptions, the stator can be considered as a conductor sheet of infinitesimal thickness placed in the inner surface of the stator. The conductor distribution is shown in (Fig.2.4). The linear current density of the winding, K_{sa}, can be written

$$K_{sa}(\theta_s) = \frac{2}{D}\frac{di_a(\theta_s)}{d\theta} \tag{2.5}$$

where $(D/2)d\theta$ is a generic elementary arc crossed by the infinitesimal current $di_a(\theta)$ [4]. Since the conductors distribution has a sinusoidal shape, the current density has a similar shape.

$$K_{sa}(\theta) = \hat{n}_d i_a \sin(p\theta_s) \tag{2.6}$$

Summing the contribution of each phase it is possible obtain the overall linear current density distribution $K_s(\theta)$

$$K_s(\theta) = \sum_{j=1}^{m} \hat{n}_d i_j(t) \sin\left[p\theta_s - (j-1)\frac{2\pi}{m}\right] \tag{2.7}$$

m is the number of phases and $i_j(t)$ is the current of the j-th phase. Considering a symmetric three-phase winding, the current can be written as a function of the position of the rotor θ_m

$$\begin{aligned} i_a &= \hat{\mathrm{I}} \cos(p\theta_m + \alpha_i^e), \\ i_b &= \hat{\mathrm{I}} \cos\left(p\theta_m + \alpha_i^e - \frac{2\pi}{3}\right), \\ i_c &= \hat{\mathrm{I}} \cos\left(p\theta_m + \alpha_i^e - \frac{4\pi}{3}\right). \end{aligned} \tag{2.8}$$

α_i^e is the angle of the current in electric degrees, p is the number of pole pairs and θ_m is the rotor position.

$$\begin{aligned} K_s(\theta) &= \hat{n}_d i_a \sin(p\theta_s) + \hat{n}_d i_b \sin\left(p\theta_s - \frac{2\pi}{3}\right) + \hat{n}_d i_c \sin\left(p\theta_s - \frac{4\pi}{3}\right), \\ &= \hat{n}_d \hat{\mathrm{I}} \left[\cos(p\theta_m + \alpha_i^e)\sin(p\theta_s) + \cos\left(p\theta_m + \alpha_i^e - \frac{2\pi}{3}\right)\sin\left(p\theta_s - \frac{2\pi}{3}\right) + \right. \\ &+ \left. \cos\left(p\theta_m + \alpha_i^e - \frac{4\pi}{3}\right)\sin\left(p\theta_s - \frac{4\pi}{3}\right)\right], \\ &= \frac{3}{2}\hat{n}_d \hat{\mathrm{I}} \sin(p\theta_s - p\theta_m - \alpha_i^e), \\ &= \hat{K}_s \sin(p\theta_s - p\theta_m - \alpha_i^e). \end{aligned} \tag{2.9}$$

$K_s(\theta)$ is the linear current density across the pole. Since that the system of sine wave currents is symmetric (2.8), also the distribution of the electric load will be symmetric and synchronous with the rotor (2.9). The maximum value is

$$\hat{K}_s = \frac{3}{2}\hat{n}_d \hat{\mathrm{I}} \tag{2.10}$$

plugging the value of $\hat{n}_d$ of equation (2.3) in (2.10), we obtain

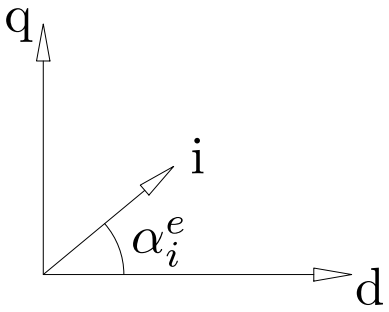

Figure 2.5: d-q refernce

$$\hat{K}_s = \frac{3k_w N \hat{I}}{\pi D} \tag{2.11}$$

using the change of reference coordinate, $\theta_s = \theta_r + \theta_m$, in equation (2.9) becomes

$$K_s(\theta_r) = \hat{K}_s \sin(p\theta_r - \alpha_i^e) \tag{2.12}$$

α_i^e represents the phase angle of the stator current in the d-q reference frame, Fig.2.5. Choosing $\alpha_i^e = 0$ means to have only d-axis current with maximum value of the linear current density distribution $\hat{K}_s(\theta_r)$ along the q-axis. Instead, impose $\alpha_i^e = \pi/2$, is equal to have only q-axis current and then minimum value of the linear current density distribution $\hat{K}_s(\theta_r)$ along the d-axis, respectively.

The electrical loading (2.12) can be decomposed in Fourier series expansion [3]

$$K_s(\theta_s) = \sum_v \hat{K}_v \sin(vp\theta_s - p\theta_m - \alpha_i^e) \tag{2.13}$$

where v is the harmonic order and $\hat{K}_v$ is the peak of electric loading harmonic of vth order. The harmonic order v can have either positive or negative sign depending of the winding, number of slots and poles. The value of this coefficient can be expressed as [2]

$$v = 6k + 1 \tag{2.14}$$

with k is an integer number, $k = 0, \pm 1, \pm 2, \ldots$.

Changing the reference frame, from the stator to the rotor (Fig.2.3),

$$p\theta_r = w_{me} t \tag{2.15}$$

the electrical loading becomes

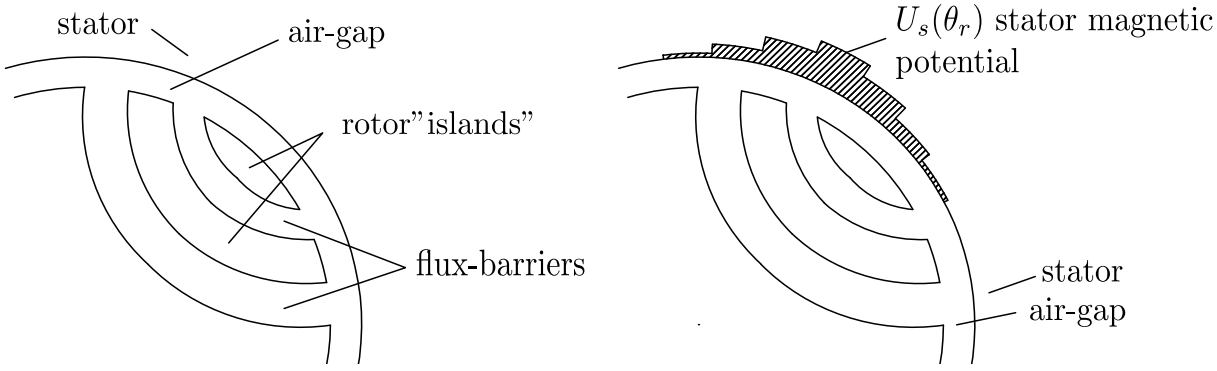

(a) Model (b) Stator magnetic potential

Figure 2.6: Stator magnetic potential

$$\begin{aligned} K_s(\theta_r) &= \sum_v \hat{K}_v \sin[vp\theta_r + (v-1)p\theta_m - \alpha_i^e] \\ &= \sum_v \hat{K}_v \sin[vp\theta_r + (v-1)w_{me}t - \alpha_i^e] \end{aligned} \tag{2.16}$$

Magnetomotive force of the stator $U_s(\theta_r)$ can be computed using Ampere's Law as shown in [2]

$$\begin{aligned} U_s(\theta_r) &= \int K_s(\theta_r)\frac{D}{2}\,d\theta_r \\ &= \sum_v -\frac{\hat{K}_v}{v}\frac{D}{2p}\cos[vp\theta_r + (v-1)w_{me}t - \alpha_i^e] \end{aligned} \tag{2.17}$$

The Fig.2.6(a) shows the geometrical motor components. It can be seen that the magnetic potential has a square distribution, Fig.2.6(b). The magnetic field of the rotor is generated as a consequence of the magnetic flux distribution. In the reluctance machine the rotor magnetic potential in the "island" is constant and proportional to the flux-barrier reluctance and the flux (Fig.2.7(a)). As it is possible to see in Fig.2.7(b) the air-gap flux density can be computed as the difference between the two magnetic potentials.

For the resolution of the analytical model some geometrical simplifications are made: the stator is replaced by infinitesimal sheet, the shape of the flux-barrier is simplified, i.e. it is assumed an equivalent reference value that describe their length and the thickness, identified equipotential magnetic axes thanks to the magnetic symmetries of the motor, which permits to consider only the complete rotor pole magnetic circuit and the iron is considered infinitely permeable.

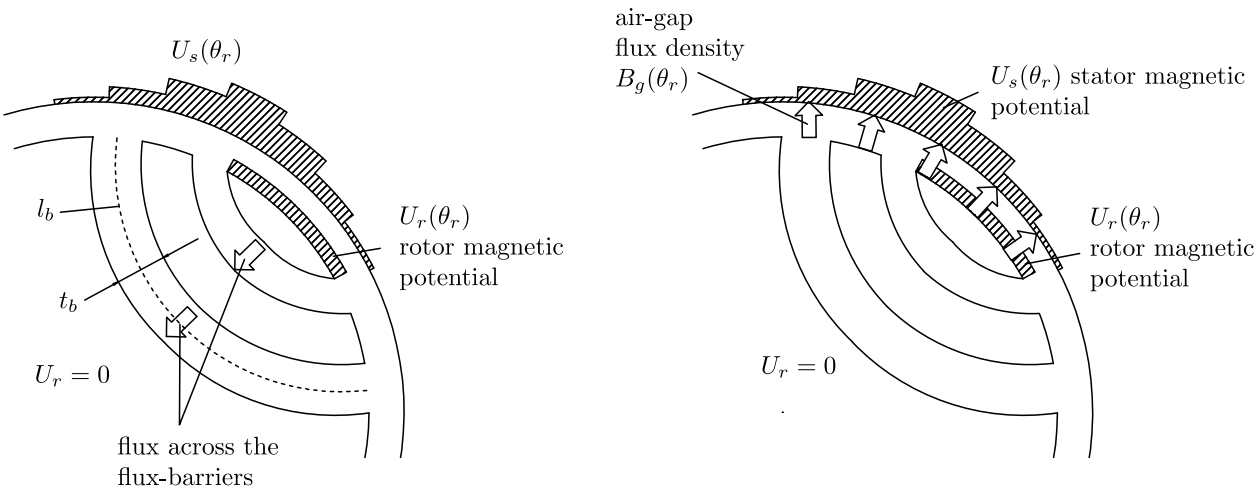

(a) Rotor magnetic potential

(b) Air-gap flux density

Figure 2.7: Rotor magnetic reaction

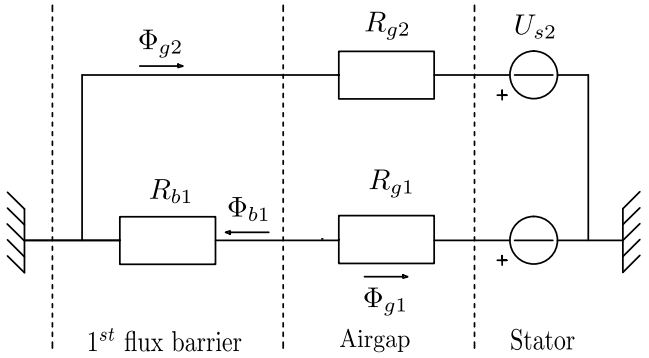

Figure 2.8: Magnetic network with one flux-barriers per pole

2.1.1 Rotor with one flux-barrier

The flux-barrier angle, θ_b, in Fig.2.1 is the half-angle of the flux-barrier (in mechanical degrees). The air-gap flux density distribution, neglecting the magnetic voltage drop in the stator iron path, is given by

$$B_g(\theta_r) = \mu_0 \frac{-U_s(\theta_r) + U_r(\theta_r)}{g} \tag{2.18}$$

The magnetic potential of the rotor is constant in the magnetic "island" and null elsewhere.

To study the configuration of the rotor with one flux-barrier per pole, it is possible to analyze the equivalent magnetic lumped-parameter network for

an SynRM (Synchronous Reluctance Motor) and the model is represent in Fig.2.8. R_{g1} represents the reluctance of the air gap over the rotor island and R_{g2} is the reluctance of the remainder air gap over the pole end.

The magnetic reluctance of the flux-barrier is given by

$$R_{b1} = \frac{t_b}{\mu_0 L_{stk} l_b} \tag{2.19}$$

where t_b and l_b are the barrier thickness and length, μ_0 is the air permeability and L_{stk} the stack length.

Integrating the air-gap flux density (2.18) the result is the magnetic flux crossing the flux-barrier

$$\phi = \phi_{b1} = \int_{\frac{\pi}{2p}-\theta_b}^{\frac{\pi}{2p}+\theta_b} -B_g(\theta_r) L_{stk} \frac{D}{2}\, d\theta_r \tag{2.20}$$

The rotor magnetic potential U_{r1} can be expressed as

$$\begin{aligned} U_{r1} &= \phi_{b1} R_b \\ &= \left[\int_{\frac{\pi}{2p}-\theta_b}^{\frac{\pi}{2p}+\theta_b} -B_g(\theta_r) L_{stk} \frac{D}{2}\, d\theta_r\right] \frac{t_b}{\mu_0 L_{stk} l_b} \\ &= \mu_0 \frac{L_{stk} D}{2g} \left[\int_{\frac{\pi}{2p}-\theta_b}^{\frac{\pi}{2p}+\theta_b} U_s(\theta_r)\, d\theta_r - 2\theta_b U_r\right] \frac{t_b}{\mu_0 L_{stk} l_b} \\ &= \frac{D}{2g}\frac{t_b}{l_b} \left[\int_{\frac{\pi}{2p}-\theta_b}^{\frac{\pi}{2p}+\theta_b} U_s(\theta_r)\, d\theta_r - 2\theta_b U_r\right] \end{aligned} \tag{2.21}$$

then

$$U_{r1}\left[1 + \frac{D}{2g}\frac{t_b}{l_b} 2\theta_b\right] = \frac{D}{2g}\frac{t_b}{l_b}\left[\int_{\frac{\pi}{2p}-\theta_b}^{\frac{\pi}{2p}+\theta_b} U_s(\theta_r)\, d\theta_r\right] \tag{2.22}$$

some dimensionless coefficients are introduced for simplify, which are in function of the geometrical parameters

$$a = \frac{\frac{D}{2g}\frac{t_b}{l_b}}{1 + \frac{D}{2g}\frac{t_b}{l_b} 2\theta_b} \tag{2.23}$$

$$k_\tau = \mu_0 \frac{D^2 L_{stk}}{g} \tag{2.24}$$

The rotor magnetic potential can be written as

$$\begin{aligned} U_{r1} &= a \int_{\frac{\pi}{2p}-\theta_b}^{\frac{\pi}{2p}+\theta_b} U_s(\theta_r)\, d\theta_r \\ &= a \sum_v \int_{\frac{\pi}{2p}-\theta_b}^{\frac{\pi}{2p}+\theta_b} -\frac{\hat{K}_v}{v}\frac{D}{2p}\cos[vp\theta_r + (v-1)w_{me}t - \alpha_i^e] \\ &= a \sum_v -\frac{\hat{K}_v}{v}\frac{D}{2p}\frac{1}{vp}\sin[vp\theta_r + (v-1)w_{me}t - \alpha_i^e]\Bigg|_{\frac{\pi}{2p}-\theta_b}^{\frac{\pi}{2p}+\theta_b} \end{aligned} \tag{2.25}$$

the argument inside the trigonometric function (2.25) can be grouped in an unique term (2.26)

$$\lambda_v = \frac{v\pi}{2} + (v-1)w_{me}t - \alpha_i^e \tag{2.26}$$

the equation (2.25) can be written as

$$U_{r1} = -aD \sum_v \frac{\hat{K}_v}{(vp)^2}\cos\lambda_v \sin(vp\theta_b) \tag{2.27}$$

It is possible to obtain the torque expression from the integration of the Lorentz's force density [2] along the air-gap surface, multiplied by the radius $D/2$

$$\begin{aligned} \tau_m &= -\frac{D}{2}\int_0^{2\pi} B_g(\theta_r)K_s(\theta_r)\frac{DL_{stk}}{2}\, d\theta_r \\ &= -\frac{D}{2}\int_0^{2\pi} \mu_0 \frac{-U_s(\theta_r)+U_r}{g}K_s(\theta_r)\frac{DL_{stk}}{2}\, d\theta_r \\ &= \frac{\mu_0}{g}\frac{D^2L_{stk}}{4}\left[\underbrace{\int_0^{2\pi} Us(\theta_r)K_s(\theta_r)\, d\theta_r}_{A} + \underbrace{\int_0^{2\pi} -Ur(\theta_r)K_s(\theta_r)\, d\theta_r}_{B}\right] \end{aligned} \tag{2.28}$$

The first part of the integral (2.28), A, is null since $U_s(\theta_r)$ and $K_s(\theta_r)$ are orthogonal functions. The second part remains in (2.28), B,

$$\tau_m = \frac{\mu_0}{g}\frac{D^2L_{stk}}{4}\int_0^{2\pi} -Ur(\theta_r)K_s(\theta_r)\, d\theta_r \tag{2.29}$$

It is important to note that $U_r(\theta_r)$ is a function piece-wise defined, only in the intervals $(\pi/2p - \theta_b, \pi/2p + \theta_b)$ and $(3\pi/2p - \theta_b, 3\pi/2p + \theta_b)$ assumes a value and null elsewhere, also has opposite value under every other pole.

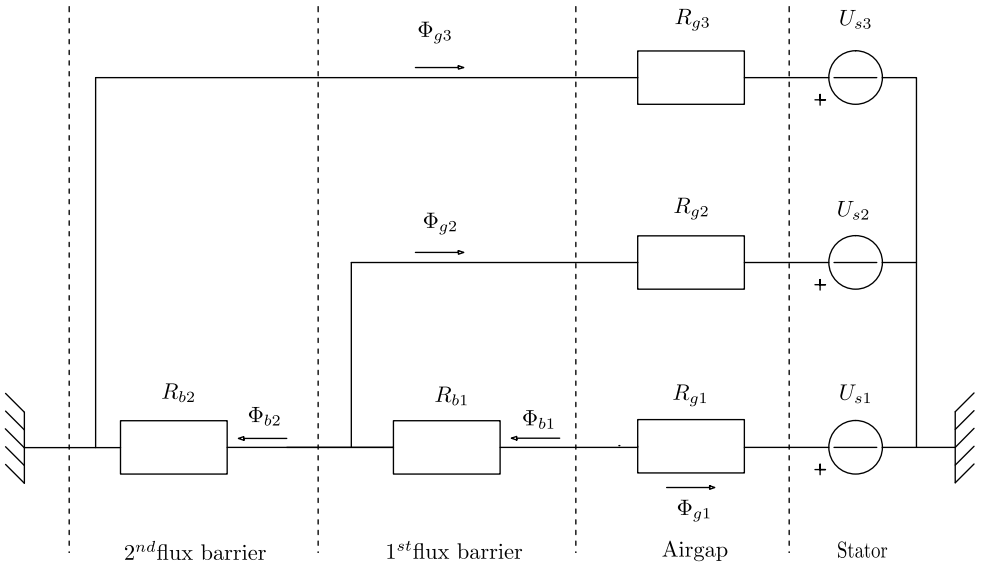

Figure 2.9: Magnetic network with two flux-barriers per pole

Only two poles are considered thanks the symmetry of the motor, it is only necessary multiply the result by the number of the pole pairs p.

After some manipulation the expression of the torque is

$$\tau_m = \frac{\mu_0}{g}\frac{D^2 L_{stk}}{4} U_{r1}(-2p) \int_{\frac{\pi}{2p}-\theta_b}^{\frac{\pi}{2p}+\theta_b} K_s(\theta_r)\, d\theta_r \tag{2.30}$$

Substituting the equations of the electric load (2.16) and the rotor magnetic potential (2.27) the torque becomes

$$\tau_m = a k_\tau \sum_v \frac{\hat{K}_v}{(vp)^2} D \cos\lambda_v \sin(vp\theta_b) \sum_\xi \frac{\hat{K}_\xi}{\xi} \sin\lambda_\xi \sin(\xi p \theta_b) \tag{2.31}$$

The two different terms of harmonics v and ξ are used to avoid confusion from the two series expansions.

2.1.2 Rotor with two flux-barriers

The analytical description of the motor with two flux-barriers is represented through the magnetic lumped-parameter network of Fig.2.9. The inner flux-barrier is named with subscript "1" and second with the subscript "2".

The electric load and the magnetic potential are defined respectively from the equation (2.6) and (2.7).

$$
\begin{aligned}
U_{r1} &= \phi_{b1} R_{b1} + U_{r2} \\
&= \int_{\frac{\pi}{2p}-\theta_{b1}}^{\frac{\pi}{2p}+\theta_{b1}} -B_g(\theta_r) \frac{L_{stk} D}{2}\, d\theta_r + U_{r2} \\
&= \int_{\frac{\pi}{2p}-\theta_{b1}}^{\frac{\pi}{2p}+\theta_{b1}} \mu_0 \frac{U_s(\theta_r) - U_{r1}}{g} \frac{L_{stk} D}{2}\, d\theta_r R_{b1} + U_{r2} \\
&= \frac{D}{2g} \frac{t_{b1}}{l_{b1}} \left[\int_{\frac{\pi}{2p}-\theta_{b1}}^{\frac{\pi}{2p}+\theta_{b1}} U_s(\theta_r)\, d\theta_r - \underbrace{\int_{\frac{\pi}{2p}-\theta_{b1}}^{\frac{\pi}{2p}+\theta_{b1}} U_s(\theta_r)\, d\theta_r}_{2\theta_{b1} U_{r1}} \right] + U_{r2} \\
&= \frac{D}{2g} \frac{t_{b1}}{l_{b1}} \int_{\frac{\pi}{2p}-\theta_{b1}}^{\frac{\pi}{2p}+\theta_{b1}} U_s(\theta_r)\, d\theta_r - \frac{D}{g} \frac{t_{b1}}{l_{b1}} \theta_{b1} U_{r1} + U_{r2} \\
&= a \int_{\frac{\pi}{2p}-\theta_{b1}}^{\frac{\pi}{2p}+\theta_{b1}} U_s(\theta_r)\, d\theta_r + b U_{r2}
\end{aligned}
\tag{2.32}
$$

and

$$
b = \frac{1}{1 + \frac{D}{2g} \frac{t_{b1}}{l_{b1}} 2\theta_{b1}} \tag{2.33}
$$

The two coefficients a (2.23) and b (2.33) are dimensionless and functions of the motor geometry. The magnetic potential of the outer island is computed by means of the flux crossing through the flux-barrier, wich is

$$
\begin{aligned}
U_{r2} &= \phi_{b2} R_{b2} \\
&= \left[\phi_{b1} + \int_{\frac{\pi}{2p}-\theta_{b2}}^{\frac{\pi}{2p}-\theta_{b1}} -B_g(\theta_r) \frac{L_{stk} D}{2}\, d\theta_r + \int_{\frac{\pi}{2p}+\theta_{b1}}^{\frac{\pi}{2p}+\theta_{b2}} -B_g(\theta_r) \frac{L_{stk} D}{2}\, d\theta_r \right] R_{b2} \\
&= \left[\frac{U_{r1} - U_{r2}}{R_{b1}} + \int_{\frac{\pi}{2p}-\theta_{b2}}^{\frac{\pi}{2p}-\theta_{b1}} \mu_0 \frac{U_s(\theta_r) - U_{r2}}{g} \frac{L_{stk} D}{2}\, d\theta_r + \right. \\
&\left. + \int_{\frac{\pi}{2p}+\theta_{b1}}^{\frac{\pi}{2p}+\theta_{b2}} \mu_0 \frac{U_s(\theta_r) - U_{r2}}{g} \frac{L_{stk} D}{2}\, d\theta_r \right] R_{b2} \\
&= \left[\frac{U_{r1} - U_{r2}}{t_{b1}} l_{b1} + \frac{D}{2g} \left(\int_{\frac{\pi}{2p}-\theta_{b2}}^{\frac{\pi}{2p}-\theta_{b1}} (U_s(\theta_r) - U_{r2})\, d\theta_r + \right. \right. \\
&\left. \left. + \int_{\frac{\pi}{2p}+\theta_{b1}}^{\frac{\pi}{2p}+\theta_{b2}} (U_s(\theta_r) - U_{r2})\, d\theta_r \right) \right] \frac{t_{b2}}{l_{b2}}
\end{aligned}
\tag{2.34}
$$

Substituting U_{r1} (2.32) in the equation (2.34) and assuming U_{r2} constant, the result is

$$\begin{aligned} U_{r2} &= U_{r2}\frac{t_{b2}}{l_{b2}}\left[(b-1)\frac{l_{b1}}{t_{b1}} - \frac{D}{2g}2(\theta_{b2}-\theta_{b1})\right] + \frac{t_{b2}}{l_{b2}}\left[a\frac{l_{b1}}{t_{b1}}\int_{\frac{\pi}{2p}-\theta_{b1}}^{\frac{\pi}{2p}+\theta_{b1}} U_s(\theta_r)\,d\theta_r + \right. \\ &\left. + \frac{D}{2g}\left(\int_{\frac{\pi}{2p}-\theta_{b2}}^{\frac{\pi}{2p}-\theta_{b1}} U_s(\theta_r)\,d\theta_r + \int_{\frac{\pi}{2p}+\theta_{b1}}^{\frac{\pi}{2p}+\theta_{b2}} U_s(\theta_r)\,d\theta_r\right)\right] \\ &= c\int_{\frac{\pi}{2p}-\theta_{b1}}^{\frac{\pi}{2p}+\theta_{b1}} U_s(\theta_r)\,d\theta_r + \\ &+ d\left(\int_{\frac{\pi}{2p}-\theta_{b2}}^{\frac{\pi}{2p}-\theta_{b1}} U_s(\theta_r)\,d\theta_r + \int_{\frac{\pi}{2p}+\theta_{b1}}^{\frac{\pi}{2p}+\theta_{b2}} U_s(\theta_r)\,d\theta_r\right) \end{aligned} \tag{2.35}$$

Also the coefficients c and d are dimensionless and they depend from geometrical parameters.

$$c = \frac{a\frac{l_{b1}}{t_{tb1}}\frac{t_{b2}}{l_{b2}}}{1-(b1)\frac{l_{b1}}{tb1}\frac{t_{b2}}{l_{b2}} + \frac{D}{g}\frac{t_{b2}}{l_{b2}}(\theta_{b2}-\theta_{b1})} \tag{2.36}$$

$$d = \frac{\frac{D}{2g}\frac{t_{b2}}{l_{b2}}}{1-(b1)\frac{l_{b1}}{tb1}\frac{t_{b2}}{l_{b2}} + \frac{D}{g}\frac{t_{b2}}{l_{b2}}(\theta_{b2}-\theta_{b1})} \tag{2.37}$$

The integral of the magnetic potential $U_s(\theta_r)$ from the air-gap to the inner flux-barrier is

$$S_1 = \int_{\frac{\pi}{2p}-\theta_{b1}}^{\frac{\pi}{2p}+\theta_{b1}} U_s(\theta_r)\,d\theta_r = \sum_v -\frac{\hat{K}_v}{(vp)^2}D[\cos(\lambda_v)\sin(vp\theta_{b1})] \tag{2.38}$$

λ_v is described in the equation (2.26). The integral between the inner and the outer flux-barrier is

$$\begin{aligned} S_2 &= \int_{\frac{\pi}{2p}-\theta_{b2}}^{\frac{\pi}{2p}-\theta_{b1}} U_s(\theta_r)\,d\theta_r + \int_{\frac{\pi}{2p}+\theta_{b1}}^{\frac{\pi}{2p}+\theta_{b2}} U_s(\theta_r)\,d\theta_r \\ &= \sum_v -\frac{\hat{K}_v}{(vp)^2}D\cos(\lambda_v)[\sin(vp\theta_{b2}) - \sin(vp\theta_{b1})] \end{aligned} \tag{2.39}$$

U_{r2} results

$$\begin{aligned} U_{r2} &= cS_1 + dS_2 \\ &= \sum_v \frac{\hat{K}_v}{(vp)^2} D \left[-c\cos(\lambda_v)\sin(vp\theta_{b1}) - d\cos(\lambda_v)[\sin(vp\theta_{b2}) - \sin(vp\theta_{b1})] \right] \\ &= -\sum_v \frac{\hat{K}_v}{(vp)^2} D\cos(\lambda_v) \left[(c-d)\sin(vp\theta_{b1}) + d\sin(vp\theta_{b2}) \right] \end{aligned} \tag{2.40}$$

from the equation (2.32) it is possible to obtain the rotor magnetic potential U_{r1}

$$\begin{aligned} U_{r1} &= a\int_{\frac{\pi}{2p}-\theta_{b1}}^{\frac{\pi}{2p}+\theta_{b1}} U_s(\theta_r)\, d\theta_r \\ &= -a\sum_v \frac{\hat{K}_v}{(vp)^2} D\cos(\lambda_v)\sin(vp\theta_{b1}) + \\ &+ b\sum_v \frac{\hat{K}_v}{(vp)^2} D\cos(\lambda_v)[(c-d)\sin(vp\theta_{b1}) + d\sin(vp\theta_{b2})] \\ &= -\sum_v \frac{\hat{K}_v}{(vp)^2} D\cos(\lambda_v)[a\sin(vp\theta_{b1}) + b(c-d)\sin(vp\theta_{b1}) + bd\sin(vp\theta_{b2})] \end{aligned} \tag{2.41}$$

rewriting the equation (2.40) and (2.41) in a more compact way, it is possible to obtain

$$U_{r1} = -\sum_v \frac{\hat{K}_v}{(vp)^2} D\rho_1 \cos(\lambda_v) \tag{2.42}$$

$$U_{r2} = -\sum_v \frac{\hat{K}_v}{(vp)^2} D\rho_2 \cos(\lambda_v) \tag{2.43}$$

the coefficients ρ_1 and ρ_2 are

$$\rho_1 = a\sin(vp\theta_{b1}) + b(c-d)\sin(vp\theta_b 1) + bd\sin(vp\theta_{b2}) \tag{2.44}$$

$$\rho_2 = (c-d)\sin(vp\theta_{b1}) + d\sin(vp\theta b2) \tag{2.45}$$

Applying the Lorentz's force Law and multiplying for the radius of the rotor $D/2$ it is possible calculate the torque [2]

$$\begin{aligned}
\tau_m &= -\frac{D}{2}\int_0^{2\pi} B_g(\theta_r)K_s(\theta_r)\frac{D}{2}L_{stk}\,d\theta_r = \frac{\mu_0 D^2}{4g}L_{stk}\int_0^{2\pi} -U_r(\theta_r)K_s(\theta_r)\,d\theta_r \\
&= \frac{k_t}{4}(-p)\left[\int_{\frac{\pi}{2p}-\theta_{b2}}^{\frac{\pi}{2p}-\theta_{b1}} U_{r2}K_s(\theta_r)\,d\theta_r + \int_{\frac{\pi}{2p}-\theta_{b1}}^{\frac{\pi}{2p}+\theta_{b1}} U_{r1}K_s(\theta_r)\,d\theta_r + \int_{\frac{\pi}{2p}+\theta_{b1}}^{\frac{\pi}{2p}+\theta_{b2}} U_{r2}K_s(\theta_r)\,d\theta_r\right] \\
&= -\frac{k_\tau p}{2}\left[\int_{\frac{\pi}{2p}-\theta_{b2}}^{\frac{\pi}{2p}-\theta_{b1}}\left(-\sum_v \frac{\hat{K}_v}{(vp)^2}D\rho_2\cos(\lambda_v)\right)\sum_\xi \hat{K}_\xi \sin\lambda_\xi\,d\theta_r + \dots\right] \\
&= \frac{k_\tau p}{2}\left[\sum_v \frac{\hat{K}_v}{(vp)^2}\cos\lambda_v \sum_{xi}\hat{K}_\xi\left(\rho_2\int_{\frac{\pi}{2p}-\theta_{b2}}^{\frac{\pi}{2p}-\theta_{b1}}\sin\lambda_\xi\,d\theta_r + \rho_1\int_{\frac{\pi}{2p}-\theta_{b1}}^{\frac{\pi}{2p}+\theta_b 1}\sin\lambda_\xi\,d\theta_r + \right.\right. \\
&\left.\left. + \rho_2\int_{\frac{\pi}{2p}+\theta_{b1}}^{\frac{\pi}{2p}+\theta_b 2}\sin\lambda_\xi\,d\theta_r\right)\right]
\end{aligned} \tag{2.46}$$

k_τ is defined in (2.24) and λ_ξ is

$$\lambda_\xi = \frac{\xi\pi}{2} + (\xi-1)w_{me}t - \alpha_i^e \tag{2.47}$$

The integral between the inner and the outer flux-barrier, bordered by the air gap, is equal to

$$\begin{aligned}
\int_{\frac{\pi}{2p}-\theta_{b1}}^{\frac{\pi}{2p}+\theta_{b1}} \sin\lambda_\xi\,d\theta_r &= -\frac{1}{\xi p}[\cos(\lambda_\xi + \xi p\theta_{b1}) - \cos(\lambda_\xi - \xi p\theta_{b1})] \\
&= \frac{2}{\xi p}\sin\lambda_\xi \sin(\xi p\theta_{b1})
\end{aligned} \tag{2.48}$$

$$\int_{\frac{\pi}{2p}-\theta_{b2}}^{\frac{\pi}{2p}-\theta_{b1}} \sin\lambda_\xi\,d\theta_r + \int_{\frac{\pi}{2p}+\theta_{b1}}^{\frac{\pi}{2p}+\theta_{b2}} \sin\lambda_\xi\,d\theta_r = \frac{2}{\xi p}\sin\lambda_\xi[\sin(\xi p\theta_{b2}) - \sin(\xi p\theta_{b1})] \tag{2.49}$$

and substituting in the expression of the torque (2.46)

$$\tau_m = k_\tau \sum_v \frac{\hat{K}_v}{(vp)^2}D\cos\lambda_v\left[(\rho_1-\rho_2)\sum_\xi \frac{\hat{K}_\xi}{\xi}\sin\lambda_\xi\sin(\xi p\theta_{b1}) + \rho_2\sum_\xi \frac{\hat{K}_\xi}{\xi}\sin\lambda_\xi\sin(\xi p\theta_{b2})\right] \tag{2.50}$$

2.2 Mechanical design

This model neglects the existence of any space harmonic except the fundamental. The value of the mean torque can be computed for $v = 1$ in equation (2.50).

$$\begin{aligned}\tau_{m1} &= k_\tau \hat{K}_v \frac{D}{p^2} \cos(\lambda_v)[(\rho_1 - \rho_2)\hat{K}_\xi \sin(\lambda_\xi)\sin(p\theta_b) + \rho_2 \hat{K}_{xi} \sin(\lambda_\xi)\sin(p\theta_{b2})] \\ &= k_\tau \hat{K}_v^2 \frac{D}{p^2} \cos(\lambda_v)\sin(\lambda_v)[(\rho_1 - \rho_2)\sin(p\theta_{b1}) + \rho_2 \sin(p\theta_{b2})] \\ &= k_\tau \hat{K}_v^2 \frac{D}{2p^2} \sin(2\lambda_v)[(\rho_1 - \rho_2)\sin(p\theta_{b1}) + \rho_2 \sin(p\theta_{b2})]\end{aligned} \tag{2.51}$$

The equation (2.51) is in function only of the geometric parameters (2.44) (2.45) and it is time independent. When the value of the torque is known, it is possible to calculate the value of the electric load, $\hat{K}_v$, by inverting equation (2.51) and using the following equation.

$$\tau_{m1} = \frac{P_{mec}}{2\pi \frac{f_{mec}}{60}} \tag{2.52}$$

where P_{mec} is the mechanical power [W] and f_{mec} is the rotor speed [rpm].

$$\hat{K}_{v1} = \sqrt{\frac{\tau_{m1}}{k_\tau \frac{D}{p^2} \frac{\sin(2\lambda_v)}{2}[(\rho_1 - \rho_2)\sin(p\theta_{b1}) + \rho_2 \sin(p\theta_{b2})]}} \tag{2.53}$$

the equation (2.26), λ_v, for the first harmonic becomes

$$\lambda_v = \frac{\pi}{2} - \alpha_i^e \tag{2.54}$$

Theorically, Synchronous Reluctance Motor has its best phase angle α_i^e equal to 45° [5], but with this type of winding (concentrated winding) is higher, $\alpha_i^e = 75°$. This parameter is also dependent of the degree of saturation of the iron.

Fig.2.10 represents the shape the metal with the various sizes. Where, R_{si} is the inner radius of the stator.

$$R_{si} = \frac{D}{2} \tag{2.55}$$

With the air-gap length g it is possible calculate the radius R_{ro}

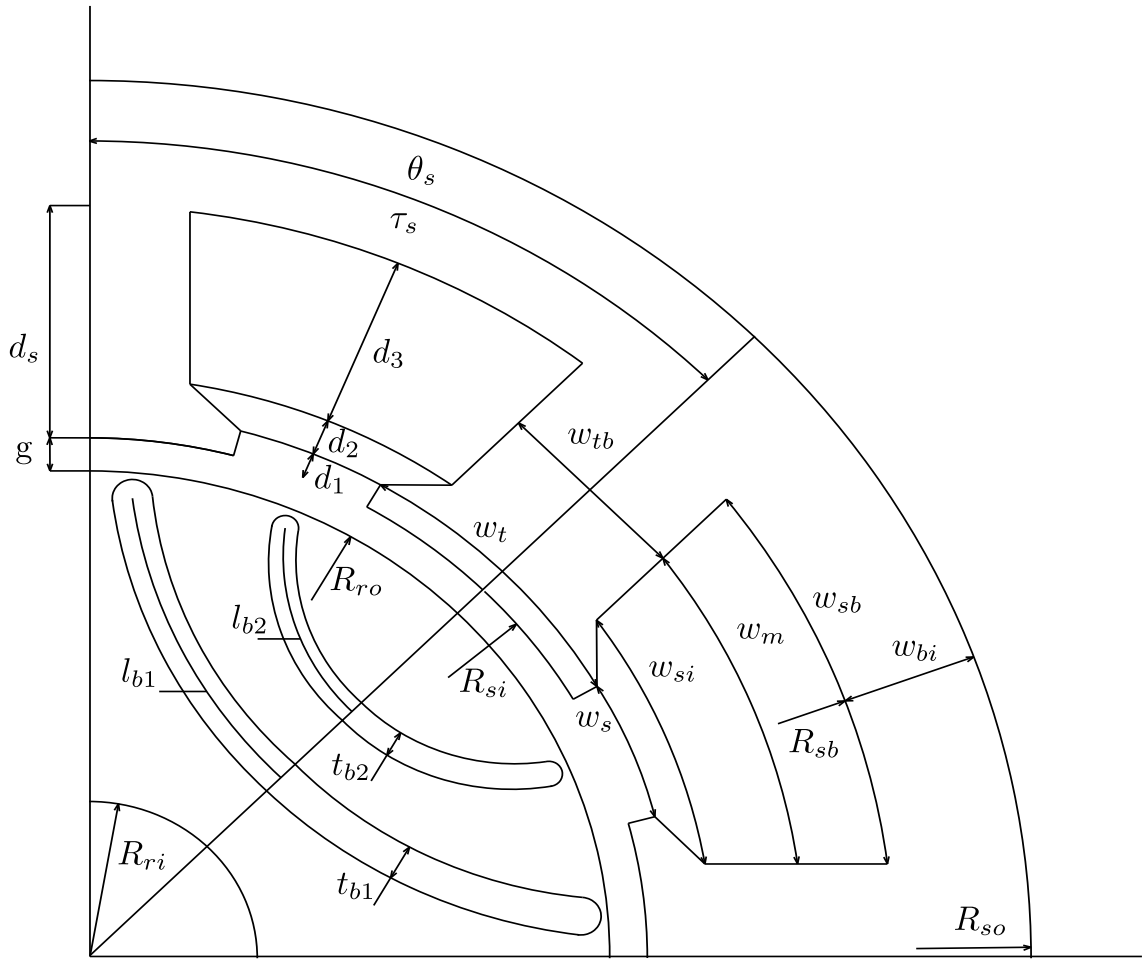

Figure 2.10: Motor shape

Table 2.1: Geometrical parameters

Size	Name
d_1	Pole shoe height
d_2	Transition height
d_3	Slot height
d_s	Total slot height
g	Air-gap lenght
l_{b1}	Length of the inner flux-barrier
l_{b2}	Length of the outer flux-barrier
R_{ri}	Shaft radius
R_{ro}	Rotor radius
R_{sb}	Stator base radius
R_{si}	Stator base radius
R_{so}	Outer stator radius
t_{b1}	Inner flux-barrier thickness
t_{b2}	Outer flux-barrier thickness
τ_p	Pole pitch at the inside radius
τ_s	Angular slot pitch
θ_p	Pole pitch angle
θ_s	Slot pitch angle
w_{b1}	Back iron width
w_m	Mean width of the slot
w_s	Slot opening
w_{sb}	External slot width
w_{si}	Internal slot width
w_t	Polar shoe width
w_{tb}	Teeth width

$$R_{ro} = R_{si} - g \tag{2.56}$$

Using the peak value of the electrical load $\hat{K}_v$, it is possible to obtain the rotor and the stator magnetic potential U_{r1} (2.42) U_{s1} (2.17). Subtracting the peak values of the magnetic potentials and applying the equation (2.18) the result is peak value of the flux density at the air-gap B_g. The efficiency target, η_{target}, can be written as follow

$$P_{in} = \frac{P_{mec}}{\eta_{target}} \tag{2.57}$$

This type of electric motor is characterized by a low value of power factor. The power factor, $\cos(\varphi)$, is the angle between current and voltage. This value is around 74°. For the calculation of the phase current, I_{ph}, is necessary to know the maximum phase voltage that can be achieved by the inverter. This value is $E_{max} = 150V$, to obtain the maximum efficiency.

$$I_{ph} = \frac{P_{in}}{3E_{max}\cos(\varphi)} \tag{2.58}$$

The pulsation of the current f_{elec} [Hz] is obtained from the mechanical speed of the rotor, f_{mec}, and the number of pole pairs p.

$$f_{elec} = \frac{f_{mec}p}{60} \tag{2.59}$$

The flux density at the air-gap can be written as a function of the rotor position, imposed the phase angle of the current vector

$$B_g(\theta_r) = \hat{B}_g \sin(p\theta_r - \alpha_i^e) \tag{2.60}$$

Changing the reference coordinates, as in equations (2.12), (2.60) can be rewritten as a function of the stator position, θ_s, and the time, t.

$$\begin{aligned} B_g(\theta_s, t) &= \hat{B}_g \sin(p\theta_s - w_{me}t - \alpha_i^e) \\ &= \hat{B}_g \sin(p\theta_s - 2\pi f_{elec}t - \alpha_i^e) \end{aligned} \tag{2.61}$$

The flux under two stator teeth can be computed by the equation (2.61) and integrating the area formed by these teeth.

$$\begin{aligned}
\Phi(\theta_s, t) &= \int_{dS} B_g(\theta_s, t)\, dS \\
&= l_{stk} R_{ro} \int_{-\frac{\pi}{Q}}^{\frac{\pi}{Q}} \hat{B}_g \sin(p\theta_s - 2\pi f_{elec} t - \alpha_i^e)\, d\theta_s \\
&= -l_{stk} R_{ro} \frac{\hat{B}_g}{p} \left[\cos(p\frac{\pi}{Q} - 2\pi f_{elec} t - \alpha_i^e) - \cos(-p\frac{\pi}{Q} - 2\pi f_{elec} t - \alpha_i^e) \right] \\
&= l_{stk} R_{ro} \frac{\hat{B}_g}{p} \left[2 \sin(-2\pi f_{elec} t - \alpha_i^e) \sin(p\frac{\pi}{Q}) \right] \\
&= 2 l_{stk} R_{ro} \frac{\hat{B}_g}{p} \sin(p\frac{\pi}{Q}) \sin(-2\pi f_{elec} t - \alpha_i^e)
\end{aligned} \tag{2.62}$$

According to Faraday's law, the electromotive force is $E(t)$

$$\begin{aligned}
E(t) &= -N_s \frac{d\Phi}{dt} \\
&= -2 N_s l_{stk} \frac{\hat{B}_g}{p} R_{ro} \sin(p\frac{\pi}{Q}) \cos(-2\pi f_{elec} t - \alpha_i^e)(-2\pi f_{elec}) \\
&= N_s l_{stk} \frac{\hat{B}_g}{p} R_{ro} \sin(p\frac{\pi}{Q}) 4\pi f_{elec} \cos(2\pi f_{elec} t + \alpha_i^e) \\
&= 4\pi f_{elec} N_s R_{ro} l_{stk} \frac{\hat{B}_g}{p} \sin(p\frac{\pi}{Q}) \cos(2\pi f_{elec} t + \alpha_i^e)
\end{aligned} \tag{2.63}$$

the peak value $\hat{E}$ is equal to

$$\hat{E} = 4\pi f_{elec} N_s R_{ro} l_{stk} \frac{\hat{B}_g}{p} \sin(p\frac{\pi}{Q}) \tag{2.64}$$

where N_s is the number of conductors. The number of conductors can be computed, inverting the previus equation.

$$N_s = \frac{\hat{E}}{4\pi f_{elec} l_{stk} \frac{\hat{B}_g}{p} \sin(p\frac{\pi}{Q}) R_{ro} N_{layer}} \tag{2.65}$$

Number of layers, N_{layer}, takes into account the number of layers in one slot. It is interesting to notice that the sinusoidal term of the equation (2.65) represent the winding factor k_w.

To design the slots, it is necessary calculate the effective area S_{eq}

$$S_{eq} = \frac{I_{ph} N_{layer}}{J_c} \tag{2.66}$$

S_{eq} represents the area of the slot that can be used for a concentrated winding with the current density J_c [A/m^2]. From the conductor area is easy to determine the relative radius R_{cp}. Assuming a circular section,

$$R_{cp} = \sqrt{\frac{S_{eq}}{\pi}} \tag{2.67}$$

To obtain the total slot current, I_s, it calculates the equivalent number of conductor n_{cs}

$$n_{cs} = \frac{N_{ph} N_{cond}}{Q} \tag{2.68}$$

$$I_s = N_{cond} I_{ph} \tag{2.69}$$

where N_{ph} is the number of phases. The effective area of the conductor in the slot is S_{Cuslot}

$$S_{Cuslot} = n_{cs} \pi R_{cp}^2 \tag{2.70}$$

and then the section of the slot, A_s, is

$$A_s = \frac{S_{Cuslot}}{k_{cp}} \tag{2.71}$$

where k_{cp} is the filling factor. Now, it is possible to draw the whole. The table 2.1 explains the different sizes of the stator. The width of the stator teeth w_{tb} can be derived from the relation of continuity of the flux between the air-gap and the stator per unity of length

$$w_{tb} B_{max} k_{st} = B_g \tau_s \tag{2.72}$$

$$w_{tb} = \frac{B_g \tau_s}{B_{max} k_{st}} \tag{2.73}$$

where B_{max} is the maximun value of the flux density in the iron. k_{st} is the iron stack factor. The stacking factor gives an approximate number about how much core is effective when insulation is taken into account. The slot pitch, τ_s, is the linear length between the teeth, as shows Fig.2.10.

$$\theta_s = \frac{2\pi}{Q} \tag{2.74}$$

$$\tau_s = R_{si}\theta_s \tag{2.75}$$

The width of the polar shoe w_t depends on the angular polar pitch, τ_s, and the slot opening w_s

$$w_t = \tau_s - w_s \tag{2.76}$$

The airgap flux, Φ_g, is

$$\Phi_g = \frac{B_g D L_{stk}}{p} \tag{2.77}$$

Thanks to the relation (2.77), it is possible obtain the back iron width w_{bi}.

$$w_{bi} = \frac{\Phi_g}{2B_{max} l_{stk} k_{st}} \tag{2.78}$$

where B_{max} is the maximum flux density in the iron. It is important to verify that the slot opening must be lower than the angular slot pitch. Also the pole shoe must not exceed the tooth width. The pole shoe height d_1 and the transition height d_2 are important to limit the cogging torque. To calculate d_3 one way is to solve the quadratic equation in function of the area of the slot A_s

$$w_{si} = (R_{si} + d_1 + d_2)\theta_s - w_{tb} \tag{2.79}$$

$$w_{sb} = (R_{si} + d_1 + d_2 + d_3)\theta_s - w_{tb} \tag{2.80}$$

where w_{si} and w_{sb} are the internal and external slot widths, respectively. It is possible to express the area slot in function of these variables

$$\begin{aligned} A_s &= (w_{si} + w_{sb})\frac{d_3}{2} \\ &= [(R_{si} + d_1 + d_2)\theta_s - w_{tb} + (R_{si} + d_1 + d_2 + d_3)\theta_s - w_{tb}]\frac{d_3}{2} \\ &= \frac{\theta_s}{2} d_3^2 + [(R_{si} + d_1 + d_2)\theta_s - w_{tb}] \end{aligned} \tag{2.81}$$

so it is possible to rewrite the previous equation (2.81) in the common form of a quadratic equation as $ax^2 + bx + c = 0$

$$\frac{\theta_s}{2} d_3^2 + [(R_{si} + d_1 + d_2)\theta_s - w_{tb}] - A_s = 0 \tag{2.82}$$

and solve for the variable d_3

$$d_3 = \frac{-(R_{si} + d_1 + d_2) + w_{tb} + \sqrt{((R_{si} + d_1 + d_2)\theta_s - w_{tb})^2 + 2A_s\theta_s}}{\theta_s} \quad (2.83)$$

The stator base radius R_{sb} and the outer stator radius R_{so} are calculated from the geometry as

$$R_{sb} = R_{si} + d_1 + d_2 + d_3 \quad (2.84)$$

and

$$R_{so} = R_{sb} + w_{bi} \quad (2.85)$$

Once the parametric paremeters are found, we can obtain the ohmic resistance as follow, first of all, the ohmic equation to know the ohmic resistance.

$$R_{hostate} = R_{cp}(1 + \Delta TC_{cp}) \quad (2.86)$$

where R_{cp} is the copper conductivity at 20°C ($1.68 \cdot 10^{-8}\ S/m$), ΔT is the gradient temperature (equal to $60°C$) and C_{cp} is the temperature coefficient of the copper ($3.862 \cdot 10^{-3}\ K^{-1}$). The length of the end winding L_{end} can be aproximated by

$$L_{end} = (R_{si} + R_{sb})\frac{\pi}{Q} \quad (2.87)$$

One important parameter to calculate the losses in the conductors is the phase resistance R_{ph}

$$R_{ph} = R_{hostate}N_{cond}\frac{L_{stk} + L_{end}}{S_{eq}} \quad (2.88)$$

Finally, the ohmic losses, P_{ohm}, are computed as follow,

$$P_{ohm} = N_{ph}R_{ph}I_{ph}^2 \quad (2.89)$$

To evaluate the losses in the iron P_{iron} it needs to calculate volume of the stator. These losses can be computed using the curves provided by the manufacturer as shown in (Fig.2.11). For this reason, the mass of the stator needs to be limited. The volume of the stator core is

$$Vol_{stator} = k_{st}l_{stk}Q\left[\frac{\pi}{Q}(R_{so}^2 - R_{sb}^2) + w_{tb}d_3 + w_t d_1 + d_2\frac{w_{tb} + w_t}{2}\right] \quad (2.90)$$

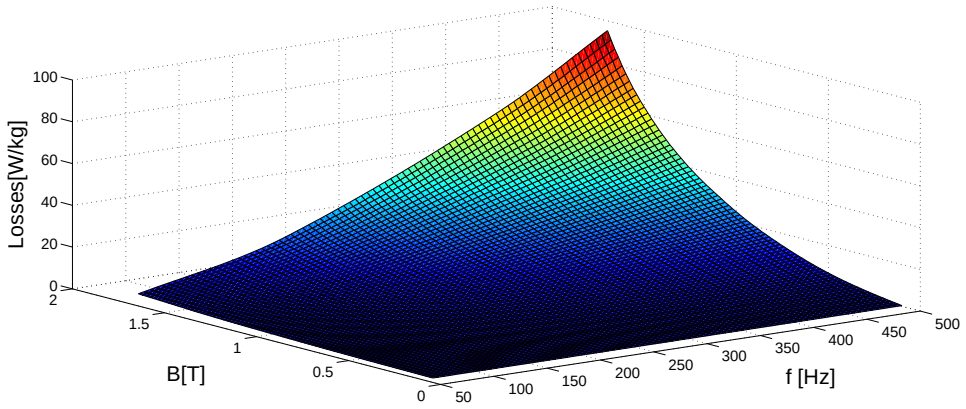

Figure 2.11: Iron losses

These losses are depending by the peak value of the flux density and the frequency. These graphs are giving the losses per unit of mass. Rotor losses are neglected since this part rotated in synchrony with the magnetic field.

$$P_{iron} = \rho_{iron} Piron_{coef} Vol_{stator} \tag{2.91}$$

where ρ_{iron} is the mass density of the iron ($7.874 \cdot 10^3\ kg/m^3$ for this type of sheet metal) and $Piron_{coef}$ is the loss coefficient $[W/kg]$ obtained from the interpolation of the loss characteristic in function of the flux density and the frequency. This data is interpolated using a piecewise spline within the limits of the information provided.

It is important to consider the windage losses [6] through the Reynolds number. These losses are function of the friction between the rotating surfaces and the surrounding gas. The rotor can be modelled as a rotating cylinder in an enclosure.

$$Re = \frac{\rho_{air} w_r R_{ro} g}{\mu_{air}} \tag{2.92}$$

where the ρ_{air} is the mass density of the air ($1.15\ kg/m^3$), μ_{air} is dynamic viscosity of the air and w_r is the angular velocity obtained by

$$w_r = \frac{2\pi f_{mec}}{60} \tag{2.93}$$

so the windage losses P_{wind} are calculated for different number of Reynolds

$$P_{wind} = \frac{0.515(\frac{g}{R_{ro}})^{0.3}}{Re^{0.5}}, Re > 10^4 \tag{2.94}$$

$$P_{wind} = \frac{0.0325(\frac{g}{R_{ro}})^{0.3}}{Re^{0.2}}, Re < 10^4 \tag{2.95}$$

knowing all the losses it is immediate the efficiency, η, calculation

$$\eta = \frac{P_{mec}}{P_{mec} + P_{wind} + P_{iron} + P_{ohm}} \tag{2.96}$$

.

Chapter 3

Fractional-slot winding

The use of a fractional number of slots and pole per phase in synchronous motors involves a series of advantages. These include high efficiency, high power density, short end turns, high slot fill factor and fault tolerance [7]. The most common configurations employed for three-phase radial-field are: the overlapped winding, and distributed (two slot/pole/phase)and concentrated (one slot/pole/phase), or nonoverlopped, i.e. concentrated with either all or alternate teeth wound. When the teeth are wound alternatively, it can be defined as single-layer and when all the teeth are wound, it can be defined as double layer.

In the overlapped distributed winding the electromotive force generally has a sinusoidal distribution. This thesis work will cover the case of nonoverlapped winding. The fault-tolerant capability is a skill that electric motors are required to have. The fault tolerance of these windings was studied in [8]. The disadvantages of this application are the slightly lower winding factor and the high harmonic contents of the magnetomotive force. For this reason is important to distinguish the main harmonic, which is the harmonic where wave lenght is equal to pole-pair pitch $2\tau_p$. This harmonic is represented by the value $v = 1$. The correct choice of p and Q can minimize the torque ripple, i.e. avoid the periodical combinations between the number of poles and slots can reduce cogging torque and torque ripple generated by harmonics. Fractional-slot winding may produce sub-harmonics, which they cause high rotor losses and unbalanced saturation among the rotor poles, that can produce high value of torque ripple mainly in motor with small air-gap.

It is interesting study a sub-class of fractional-slot windings characterized by non-overlapped coils when the angular slot pitch is near to the unity $\theta_p \simeq 1$ (Fig.3.1). It means that the number of slots Q is similar to the number of pole pairs $2p$ ($Q \simeq 2p$). The combination considered in this thesis is $Q = 6$ and $2p = 4$ [9].

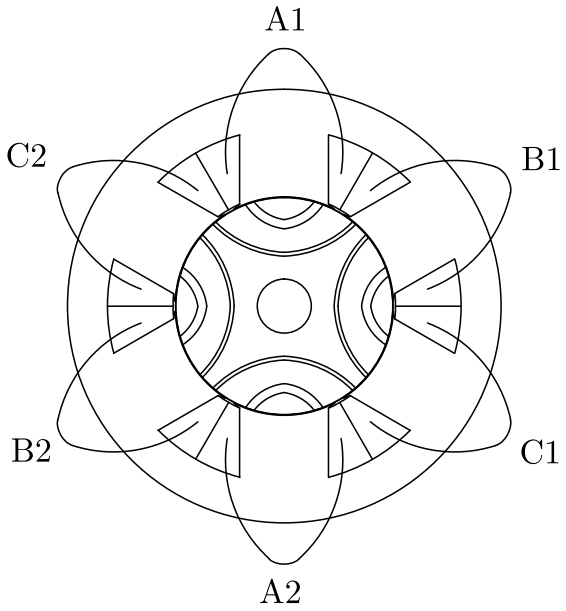

Figure 3.1: Typical stator winding

3.1 Concentrated windings

Concentrated windings have the advantage of having short end-windings. This feature minimizes the ohmic resistance of the phase and then reducing the joule losses. This is a good feature for low power household applications. This thesis presents a structures with a regular distribution of slots [10].

To determine a suitable combination of poles and slots, equation (3.1) must be verified

$$\frac{Q}{GCD(Q, 2p)} = 3k \tag{3.1}$$

where k is an integer number and GCD is the Greatest Common Divisor. For a three-phase machine the number of slots per pole q and phase is

$$q = \frac{Q}{3 \cdot 2p} \tag{3.2}$$

Electric machines, that have concentrated windings, are characterized by a value of q which is less or equal to 1/2. To determine the phases inserted in every slot, we must decompose q as the ratio of non-divisible numbers as follow, e and f

$$q = \frac{e}{f} \tag{3.3}$$

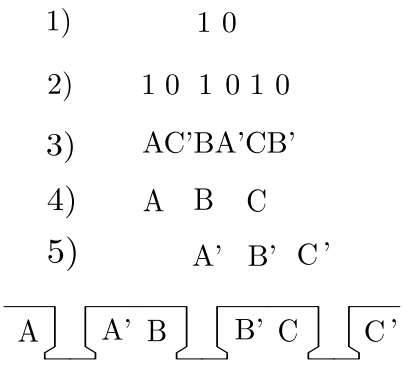

Figure 3.2: Concentrated winding of a three-phase machine with 6 slots and 4 poles

from this relation it is possible obtain a sequence of 0 and 1 specifics for the winding, where f is the total number of the coefficients, e are the numbers "1" and the others "0" are equals to $f - e$.

$$\overbrace{\underbrace{000\ldots0}_{f-e}\underbrace{111\ldots1}_{e}}^{f}$$

The winding that allows to obtain the motor with highest performance is achieved thanks the most regular distribution of "0" and "1". The sequence of f numbers has to be repeated 3 times. For the combination of Q and $2p$ considered the initial repeatable sequence is 01, which is dual to 10. The second step is to repeat the sequence 3 times as shown in Fig.3.2.

The usual phase sequence is AC'BA'CB', which is associated with the binaric sequence. The conductors with the subscript are the return conductors. In the third step, the phases positioned in correspondence with a "1" make the first layer. The second layer is obtained by reproducing and shifting the initial layer. The final structure is the pair combination of the first and the second layer.

Motors with a number of slots per pole and per phase equal to 1/2 have phases shifted 120° electric degrees. The performance of these machines are relatively low, because the winding factor of the fundamental harmonic is only 0.866. The torque ripple presents important values when the motor is loaded. For this reason this type of machine is prefered in applications of low power where the torque ripple is not an important issue.

It is possible calculate the number of pulsations N of the cogging torque with the least common multiple between Q and $2p$ in no-load condition using the following relationship [10].

$$N = LCM(Q, 2p) \tag{3.4}$$

where $N = 12, 24, 36, 48 \ldots$

Chapter 4

Genetic algorithm optimization

This chapter explains the optimization of the synchronous reluctance motor explained in the Chapters 2 and 3 with Genetic Algorithm. The aim is to optimise an objective function such as the efficiency and the material cost [11].

This part presents the combination of the analytic model with the genetic algorithm. The optimization is a computationally hard problem, for the difficulty of solve a multy-objective problem with a very big dimensionality. The big dimensionality comes from the amount of electric and geometric parameters. It is studied the case of synchronous reluctance to exemplify this optimisation technique, but it can be extended to any type of motor. The aim of the optimization is maximising or minimising an objective function related to the efficiency, motor torque, material cost or a combination of them, obtaining the motor performance. A fitness function, elaborated by the genetic algorithm, is associated to the motor performance. This algorithm emulates the natural mechanism of selection to produce motors with improved performances, taking care of manufactoring problems. On other words, the algorithm discards the worst motors in each population to select best ones.

The vector x represents the electric and geometric variables that define the synchronous reluctance motor.

$$x = (x_1, \ldots, x_n) \tag{4.1}$$

where each parameter is bounded by a maximum and minimum limit in the search space.

4.1 Description of genetic algorithm

The genetic algorithm is one of the most similar routine to the artificial intelligence. The objective is to emulate the natural selection. Optimizing the motor means explore the motor design variable space through the mechanism of reproduction, crossover and mutation with the objective to design the best motor possible.

The fitness function $F(x)$ allows to define the quality of the motor, which is related to the objective function. The genetic algorithm manipulates strings of binary digits, which represents the sets of values. The strongest strings advances at the next generation to producing more descendents.

Fig.4.1 shows the main steps of a genetic algorithm routine. First step is to define a fitness function $F(x)$. The next stage is to generat a random family of N individuals, which are codified in strings of bits (1 or 0). The third step is necessary to evaluate the population through the fitness function $F(x_i)$. The aim of this function is to predict the performance of the motor. At the next step, there is the reproduction of the best candidates until reaching N individuals. The reproduction phase is characterized by three process: $Selection$, $Crossover$ and $Mutation$. The selection process groups the old population, giving the preference to the ones having a higher fitness function.

In the crossover, two random individuals are selected and their bits are mated as shown Fig.4.2a. In the mutation stage, Fig.4.2b, one part of a string is selected and swapped from 1 to 0 and vice versa, that allows to explore new solutions in the search zone and avoiding the losses of important informations. The algorithm stops after a prefixed number of iteration max_{iter}. The indipendent variables are ten and they are shown in table 4.1. These parameters are in input of the genetic algorithm [13].

Table 4.2 shows constant values that are used in the Genetic Algorithm. This multi-objective optimization can be interpreted as a function that has as input ten free parameters and as output only two. These bits outputs represent the $efficiency$ and the $cost$ of the motor. The first aim is to minimize the cost, while the efficiency must be optimized.

The efficiency must be valuated at a power is ten times smaller as the rated power. This point is located the values of supply current and frequency defined in Table 4.3. Placing a negative sign to the cost function, it is possible to analyze the objective functions as a maximizing problem. The input vector x is constituted by a series of binary logic numbers, while the output function is realized by a set of floating numbers. In every iteration all the objectives are compared. Every candidate is computed through the analytical model presented in Chapter 2. The best candidate has the probability to be crossed, equal to P_c. The routine is implemented in Matlab, as presented in Chapter

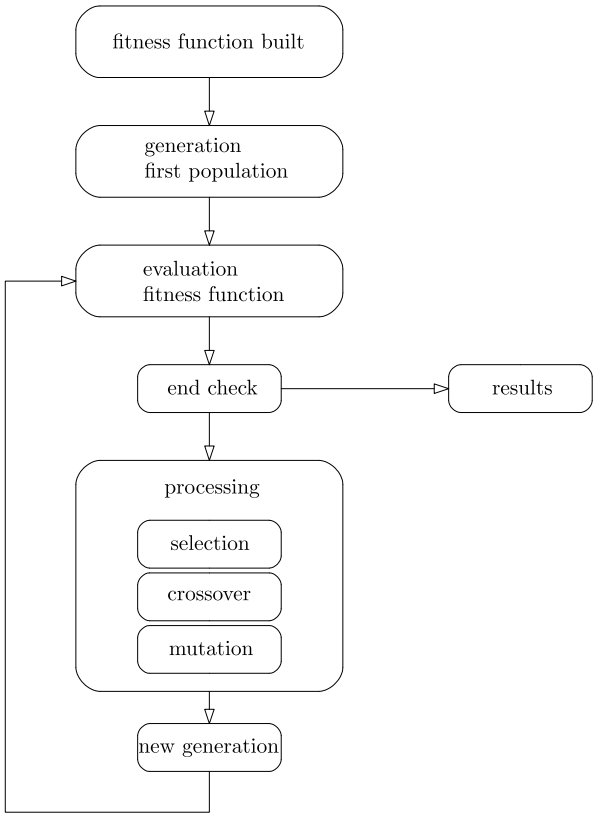

Figure 4.1: Steps of genetic algorithm

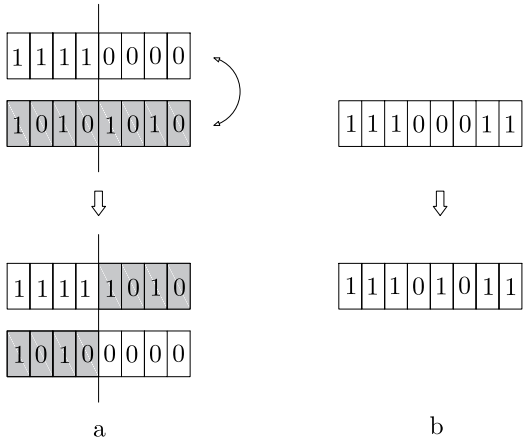

Figure 4.2: Crossover and mutation processes (*a* Crossover, *b* Mutation)

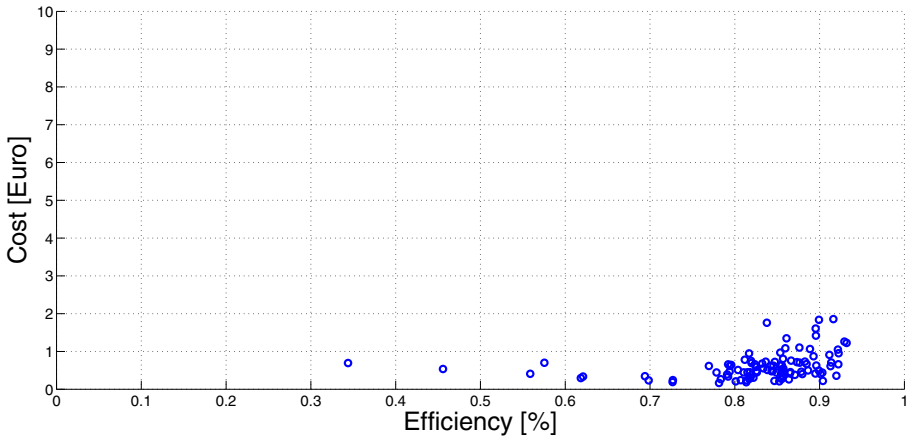

Figure 4.3: Initial population

2, in order to achieve the objective.

The coefficients necessary for the optimization are shown in Table 4.4. These parameters are chosen to allow an enough exploration in the search space.

Fig.4.3-4.4 show the initial iteration and the distribution of the solutions after hundred iterations. In the first picture, it can be seen the random distribution of the population. After many iterations, all the candidates are concentrated in a unique point. This is the result of the selection routine, only the strongest individuals remain, in terms of efficiency and price. It is worth notify that the algorithm converge in the most efficient motor.

Table 4.5 shows the geometric and electric parameters necessary for the design of the best motor of Fig.4.5. It is interesting to see the comparison of

Table 4.1: Design variables with relative limits

Variables		Search zone
Geometrical		
D	Bore diameter	$1.5{\cdot}10^{-2}{\leq}D{\leq}5{\cdot}10^{-2}[m]$
L_{stk}	Stack length	$1.5{\cdot}10^{-2}{\leq}L_{stk}{\leq}5{\cdot}10^{-2}[m]$
g	Air-gap length	$0.5{\cdot}10^{-3}{\leq}g{\leq}1{\cdot}10^{-3}[m]$
t_{b1}	Inner flux-barrier thickness	$10{\leq}t_{b1}{\leq}100[\%]$
t_{b2}	Outer flux-barrier thickness	$10{\leq}t_{b2}{\leq}100[\%]$
θ_{b1}	Inner flux-barrier angle	$10{\leq}\theta_{b1}{\leq}100[\%]$
θ_{b2}	Outer flux-barrier angle	$10{\leq}\theta_{b2}{\leq}100[\%]$
Electrical		
B_{max}	Maximum flux density in the iron	$0.1{\leq}B_{max}{\leq}1.2[T]$
J_c	Current density	$1.5{\cdot}10^{-6}{\leq}J_c{\leq}6{\cdot}10^{-6}[A/m^2]$
f_{mec}	Mechanical speed	$2{\cdot}10^3{\leq}f_{mec}{\leq}5{\cdot}10^3[rpm]$

the losses in Table 4.6, efficiency between rated and optimal point remains nearly constant. Input power and losses decrease in the same ratio, keeping a similar efficiency.

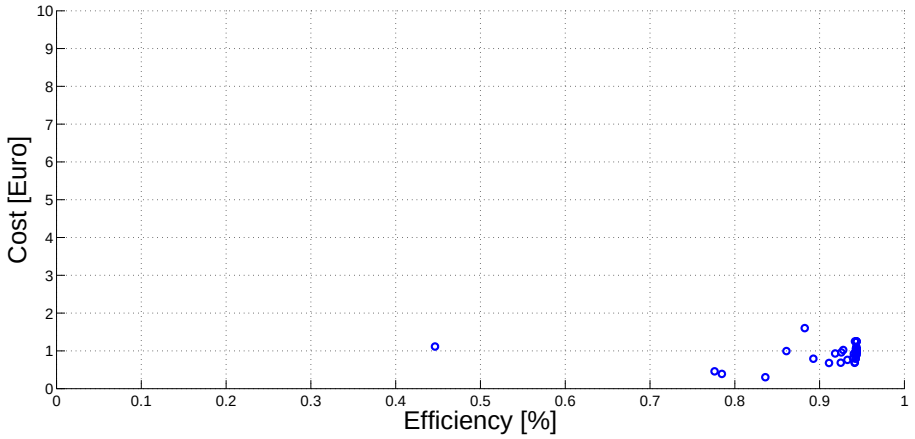

Figure 4.4: Distribution of the population after hundred iterations

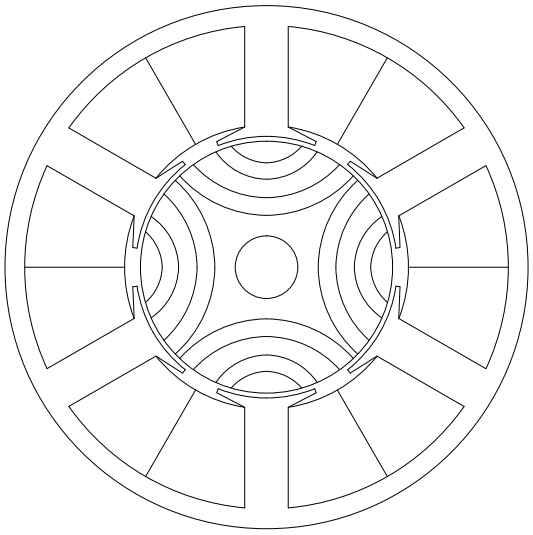

Figure 4.5: Optimized motor

Table 4.2: Constants

Parameter	Value
Ingoing power P_{in}	$100[W]$
Phase voltage E_{max}	$150[V]$
Phases number m	3
Iron stack factor k_{st}	0.9
Copper filling factor k_{cp}	0.5

Table 4.3: Optimal point

Optimal parameters	Value
Power P_{opt}	$10[W]$
Frequency f_{opt}	$f_{elec}/\sqrt{5}[Hz]$
Current I_{opt}	$I_{ph}/2[A]$

Table 4.4: Optimisation parameters

Constant	Value
Chromosome length	57
Population size	100
Tournament size	2
Maximum number of iterations	100
P_c Crossed probability	0.25
P_m Swapping probability	0.01

Table 4.5: Optimized motor

d_1	Pole shoe height	[mm]	0.5
d_2	Transition height	[mm]	1
d_3	Slot height	[mm]	14.5
d_s	Total slot height	[mm]	16
g	Air-gap length	[mm]	0.5
l_{b1}	Length of the inner flux-barrier	[mm]	25.5
l_{b2}	Length of the outer flux-barrier	[mm]	13
R_{ri}	Shaft radius	[mm]	4.5
R_{ro}	Rotor radius	[mm]	18.5
R_{sb}	Stator base radius	[mm]	35.5
R_{si}	Stator base radius	[mm]	19
R_{so}	Outer stator radius	[mm]	38.5
t_{b1}	Inner flux-barrier thickness	[mm]	2.5
t_{b2}	Outer flux-barrier thickness	[mm]	2.5
w_{bi}	Back iron width	[mm]	3
w_s	Slot opening	[mm]	5.5
w_t	Polar shoe width	[mm]	14.5
w_{tb}	Teeth width	[mm]	6.5
Q	Slot number		6
$2p$	Pole number		4
I_{ph}	Current phase	[A]	0.81
$\hat{K}_s$	Electric load peak	[A/m]	36735
N_s	Conductors number		460
T	Torque	[N/m]	0.227
f_{elec}	Electric frequency	[Hz]	139.9

Table 4.6: Comparison losses

			Rated point	Optimal point
P_{mec}	Rated power	[W]	100	10
P_{iron}	Iron losses	[W]	1.218	0.139
P_{ohm}	Ohmic losses	[W]	2.181	0.380
η	Efficiency	[%]	0.967	0.951

Chapter 5

Genetic algorithm results and FEM comparison

To evaluate the results obtained for the Genetic Algorithm, it is used a finite element software (COMSOL). Thanks to the symmetry of the motor, it is necessary to analyze half motor, reducing the computation cost, as shown Fig.5.1. The motor is divided in several domains: Ω_{co} represents the copper domain, Ω_{sh} is the area of the shaft, Ω_{ir} is the iron sheet domain and Ω_{air} is the air domain.

The machine is analysed with an impressed three phase current, as computed in table 4.5. To work in the condition of the highest torque for absolute value of current it is important to study the torque as function of the phase angle of the current α_i^e (defined in Fig.2.5) as show the graph Fig.5.6. The maximum torque value matches with a phase angle equal to 1.3 rad, or 75°.

From the analysis of the flux and the flux density, in both operating points Fig.5.2-5.3, the saturation zones match only in the tinier parts of the polar shoes. The flux does not penetrate in the shaft. The presence of harmonics is reflected on the torque variation (Fig.5.4-5.5).

The torque is evaluated trough the Maxwell stress tensor with a average value about to 0.225Nm and 0.11Nm respectively, similars to the analytical values of Table 4.5. The oscillation from the average value is equal to 56% and 54%. The value of ripple, ever high, is enough for compressor applications as long as it does not become a nuisance to the ear. As it may observed by the number of periodicity, the dominant harmonic is the sixth, which depends from the periodicity between the number of slots and poles, as previously stated.

The flux density in Fig.5.3 decreases due to the fact that supply current is employed to magnetize the iron (d-axes current decreases).

The mechanical power is shown in Fig.5.7-5.8 where the mean value is in

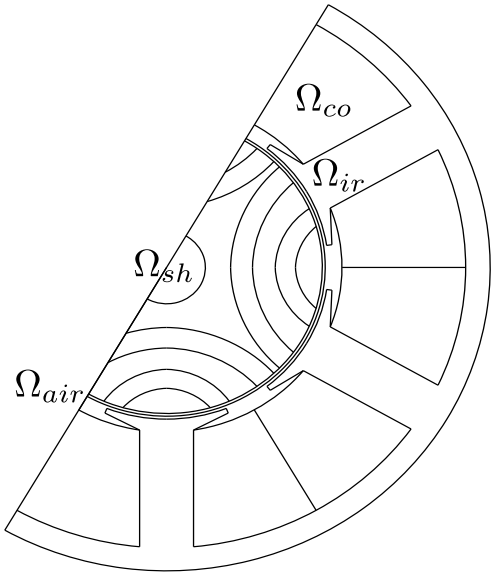

Figure 5.1: Domains of the motor

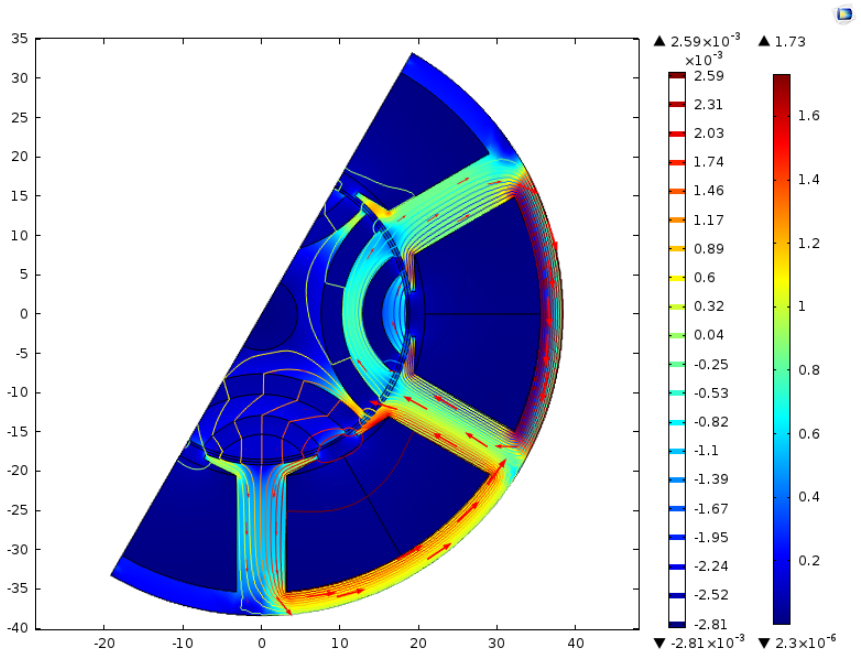

Figure 5.2: Flux density and flux lines in rated operating

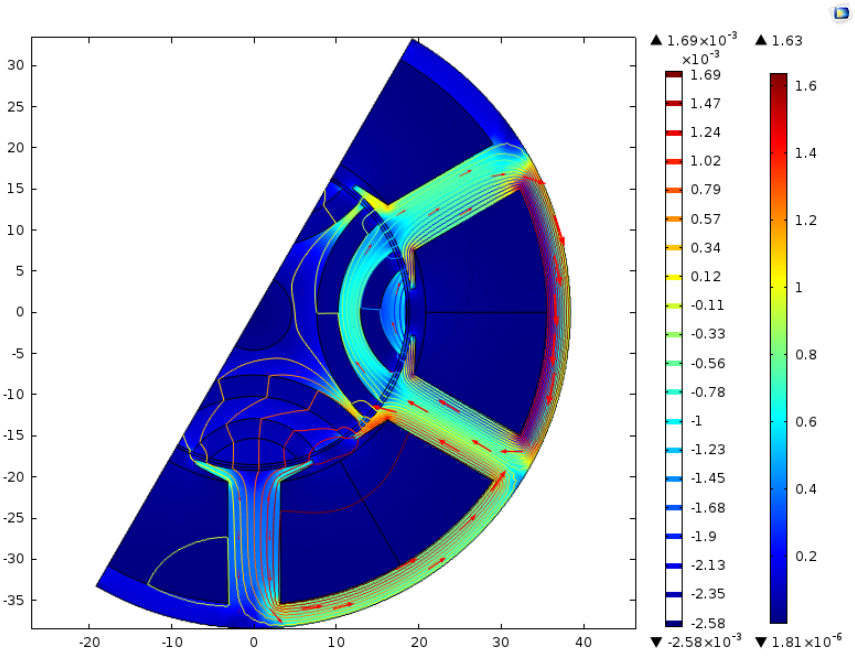

Figure 5.3: Flux density and flux lines in optimal point operating

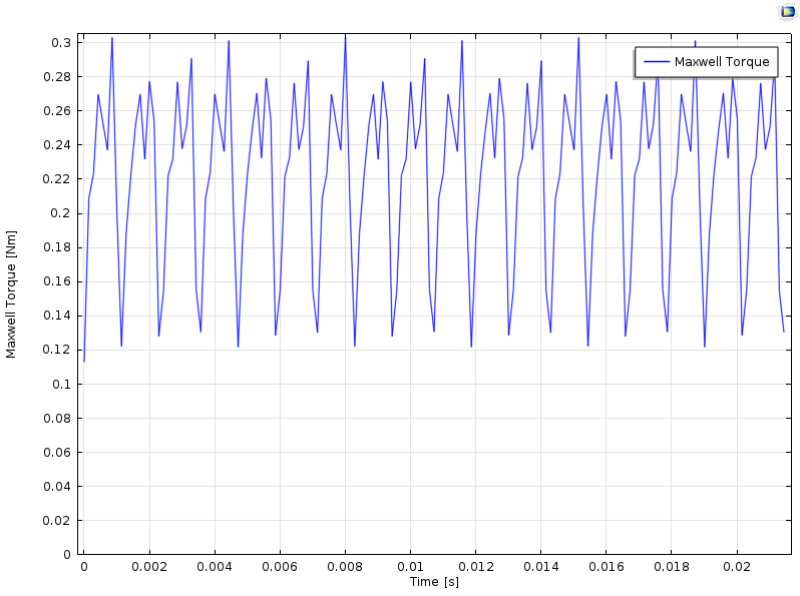

Figure 5.4: Torque expressed in function of the time calculated by the Maxwell stress tensor

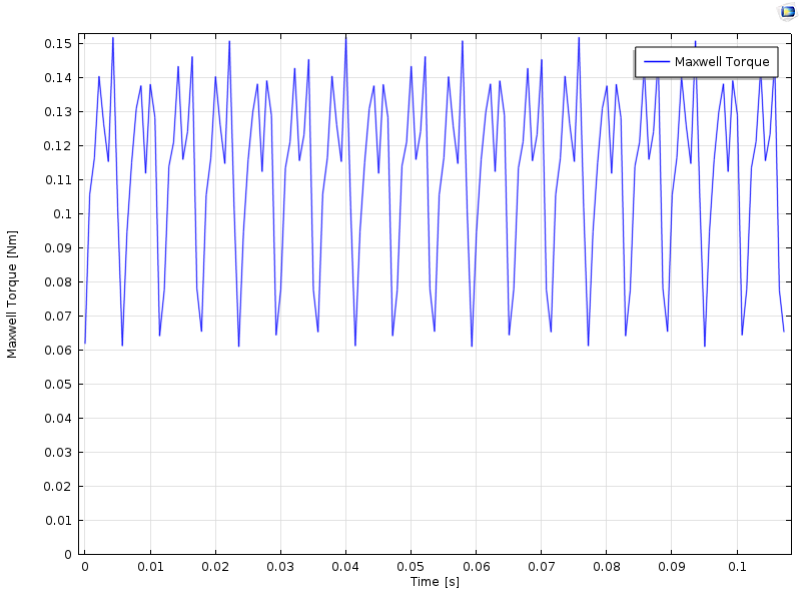

Figure 5.5: Torque expressed in function of the time calculated by the Maxwell stress tensor in the optimal point

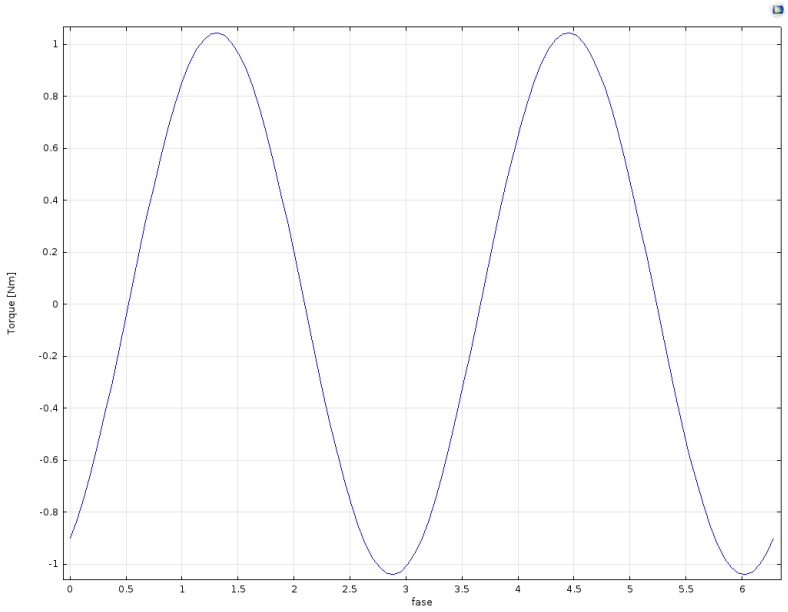

Figure 5.6: Torque expressed in function of the phase angle of the current

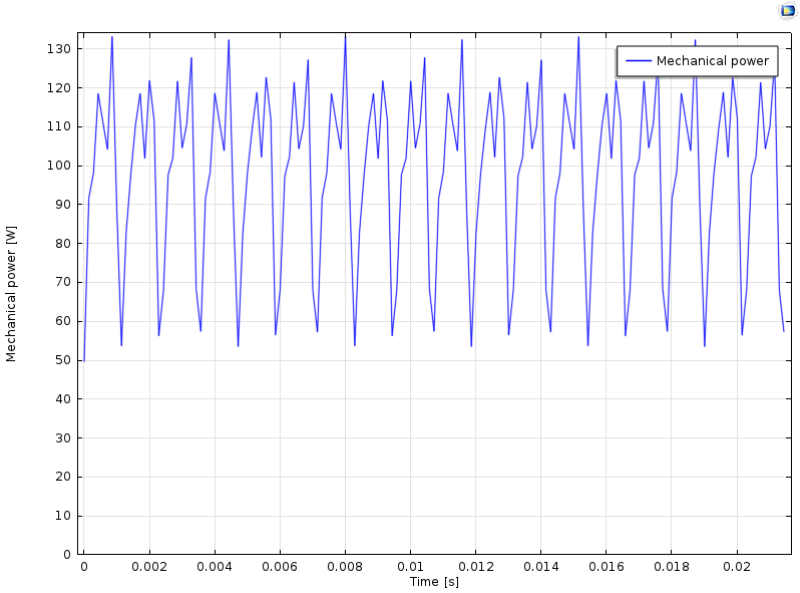

Figure 5.7: Mechanical power in function of the time

proximity of the target value and the ripples are about of 54% in both the cases.

For an accurate computation of the efficiency in different values of supply frequency and current, we need FE to compute the losses [13]. The iron and ohmic losses are considered. The conductor losses depend by the stator currents.

$$P_{ohm_{FE}} = \frac{R_{ph}}{T} \int_0^T i_{ph} i_{ph}^T \, dt = \frac{R_{ph}}{T} (i_{ph}, i_{ph}^T) \tag{5.1}$$

The phase resistance, R_{ph}, is computed in the equation (2.88). The current phase i_{ph} is a vector in time integration form with amplitude equal to equation (2.58). The iron losses, $P_{iron_{FE}}$, are computed as a sum of differents terms,

$$P_{iron_{FE}} = P_h + P_{ed} + P_{ex} \tag{5.2}$$

where P_h are the hysteresis losses, P_{ed} are the eddy current losses and P_{ex} are the losses due to movement of domain blocks inside the iron [14]. These losses are defined as follow

$$P_h = c_h \int_0^T \int_{\Omega_{ir}} H \cdot \frac{dB}{dt} d\Omega_{ir} \, dt \tag{5.3}$$

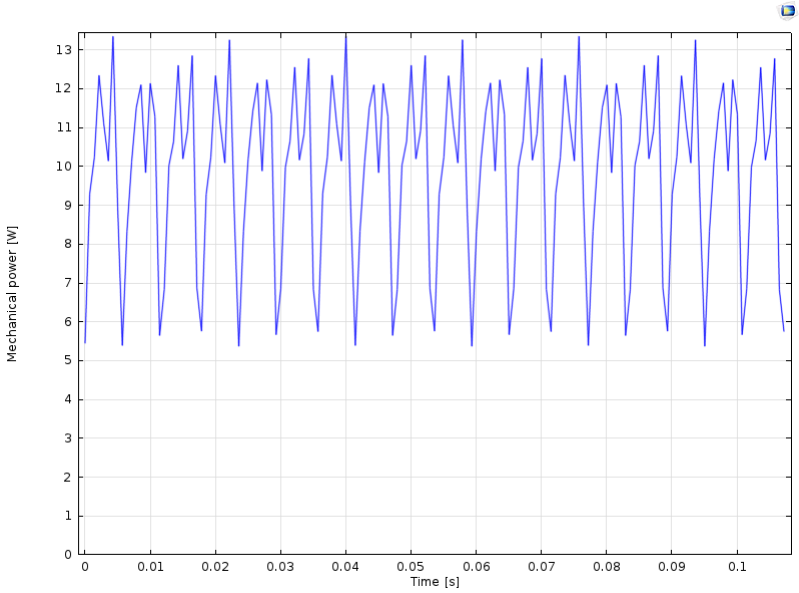

Figure 5.8: Mechanical power in function of the time

$$P_{ed} = \frac{\sigma L_{stk}^2 N_{stk}}{12T} \int_0^T \int_{\Omega_{ir}} \left(\frac{dB}{dt}\right)^2 d\Omega_{ir}\, dt \tag{5.4}$$

$$P_{ex} = \frac{c_{ex}}{T} \int_0^T \int_{\Omega_{ir}} \left|\frac{dB}{dt}\right|^{1.5} d\Omega_{ir}\, dt \tag{5.5}$$

where the coefficients c_h and c_{ex} are interpolated using optimization algorithms in the iron losses curve, Fig.2.11. The number of iron stacks is expressed by N_{stk}. The losses in the iron parts of the rotor must be reformulated because the magnetic fields are attached to the spatial frame of reference of the FE model. The time derivatice equation becomes

$$\frac{dB}{dt} = \frac{dB}{dt} + \frac{dB}{dx}\frac{dx}{dt} = \frac{dB}{dt} + \nabla^x B \cdot v \tag{5.6}$$

Windage losses are neglected in this model.

Fig.5.9-5.11 show the trends of the different contributions of the losses in function of the frequency and the current phase. It is interesting to notify that the trend of the losses are similar in both the 3 graph. The losse are improved at the growing of the supply current and frequency.

Knowing the mechanical power it is possible to obtain the efficiency map of Fig.5.12. In the efficiency map, it can be seen that in both conditions of work, rated and optimal power, the efficiency of the motor is higher than the target equal to 95%.

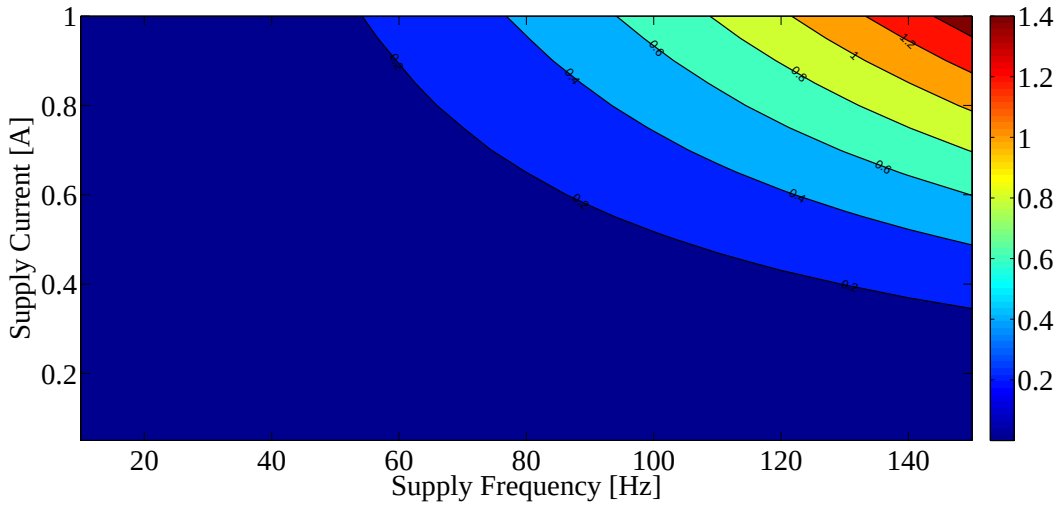

Figure 5.9: Eddy current loss

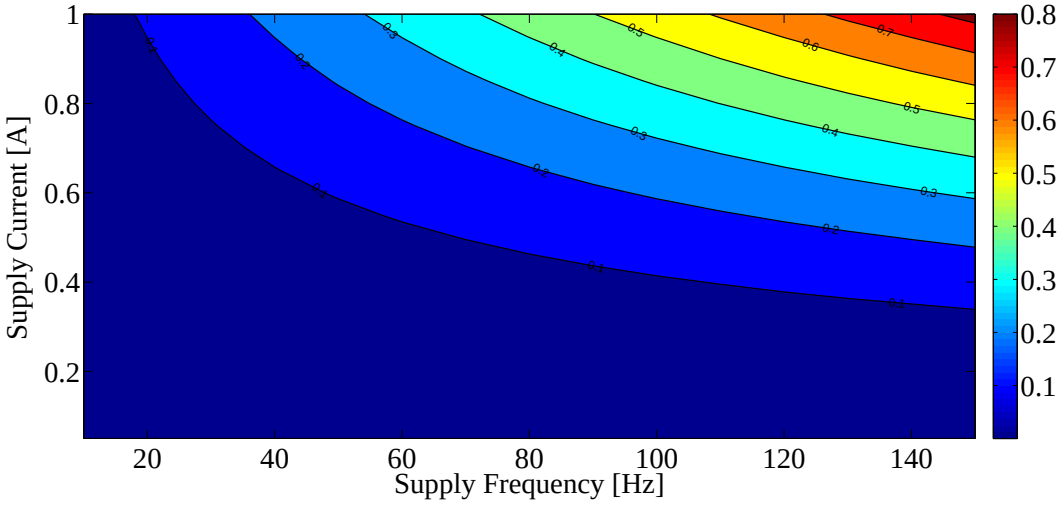

Figure 5.10: Hysteresis losses

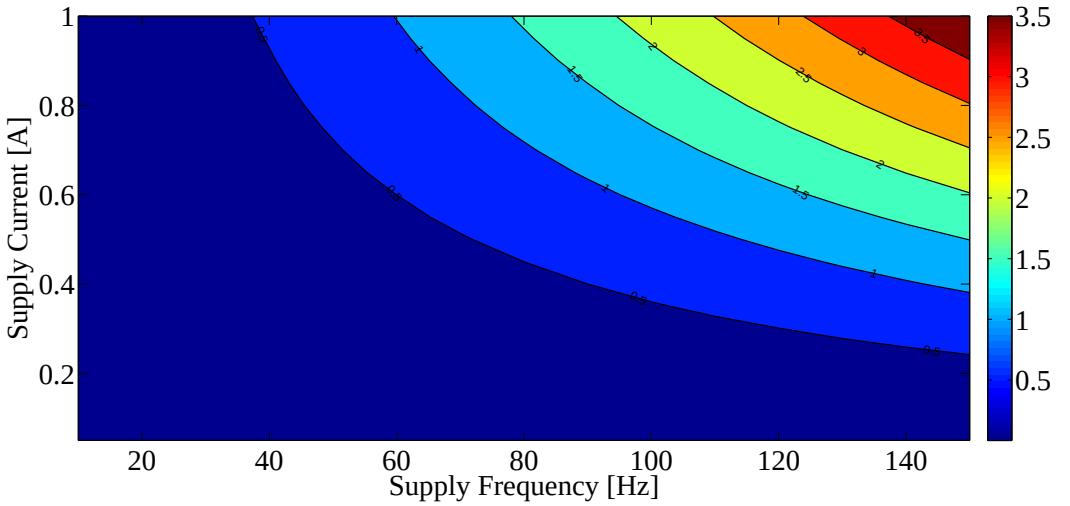

Figure 5.11: Excess Losses

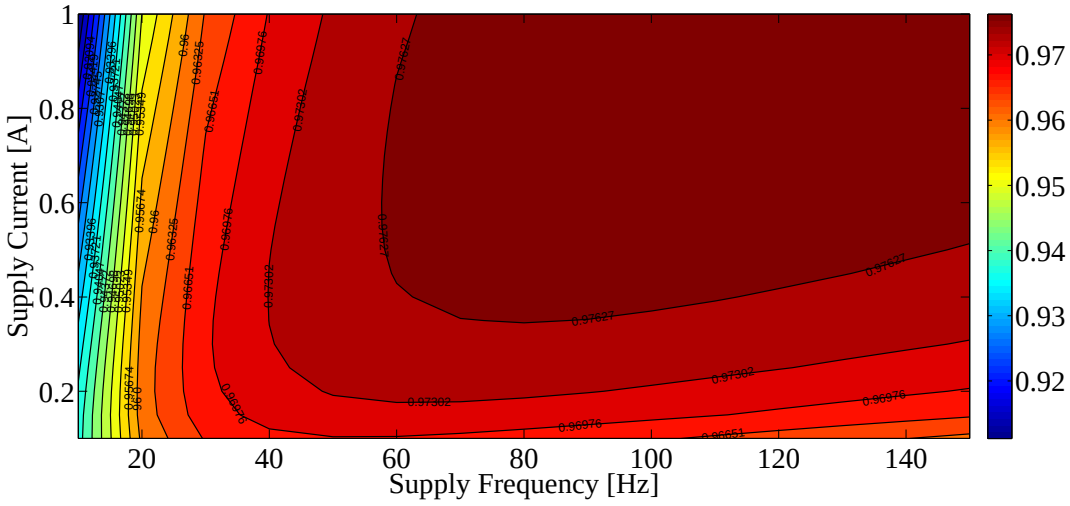

Figure 5.12: Efficiency map

Chapter 6

Conclusions

The target of the project has been achieved by conducting a detailed study on the features and performance of the synchronous reluctance motor. Some of the design parameters an their effect on motor performance have been identified by doing finite element analysis simulations. Prior to the computation of the motor using FE, the optimization of an analytical model has been performed. In the optimization of the motor, a good magnetic design can be achieved only with a analytical model, i.e. without a numerical analysis. Although, the finite element simulation is necessary to consider the nonlinear behaviors of the material.

In the second chapter was performed an analytical model to determine the contribute of the motor shape in the performance. The variables are the dimensions of the flux-barriers, of the rotor and some electric parameters as the current density and the maximum flux density in the iron. The motor analyzed is with fractional slots, in this case with four poles, six slots and transversely laminated. An algorithm allows to obtain an optimized geometry with two flux-barriers.

The third chapter explaines the factors for the choose of this type of winding with its strengths, weaknesses and limitations. The concentrated winding allows to reduce the length of the conductors, using less material and decreasing the ohmic losses. Even though it involves a high harmonic content.

During the fifth chapter, a worthy verification of the analytical results has been presented. The results of this thesis show that the Synchronous Reluctance Motor, taken into account, is characterized by high efficiency in a wide operating zone and low materials cost. In spite of their poor value of power factor.

Bibliography

[1] P. Alotto, M. Barcaro, N. Bianchi, and M. Guarnieri, "Optimization of interior PM motors with machaon rotor flux barriers," *IEEE, Transaction on Magnetics*, vol.47, no. 5, pp. 958-961, May 2011.

[2] N. Bianchi, S. Bolognani, D. Bon, M. Dai Pré, "Rotor flux-barrier design for torque ripple reduction in synchronous reluctance and PM-assisted synchronous reluctance motors," *IEEE, Trans. on Industry Applications*, vol. 45, no. 3, pp. 921-928, May/June 2009.

[3] N. Bianchi, S. Bolognani, D. Bon, M. Dai Pré, "Torque harmonic compensation in a synchronous reluctance motor," *IEEE, Transaction on Energy Conversion*, vol. 23, no. 2, pp. 466-473, June 2008.

[4] N. Bianchi, "Analysis of the IPM motor-Part I. Analytical approach in design, anlysis, and control of interior PM synchronous machines," in *Conf. Rec. IEEE IAS Annu. Meeting*, N. Bianchi and T. M. Jahns, Eds. Seattle, WA, Oct.3, 2005, pp. 3.1-3.33. IEEE IAS Tutorial Course Notes, CLEUP (info@cleup.it).

[5] S. Bolognani, "Capitolo 5 - Motore brushless sinusoidale" course notes of Electric Drives.

[6] J. Pyrhönen, T.Jokinen, V. Hrabovcová, "Design of Rotating Electrical Machines"

[7] A. M. EL-Refaie, "Fractional-Slot Concentrated-Windings Synchronous Permanet Magnet Machines: Opportunities and Challenges" *IEEE, Transactions on Industrial Electronics*, vol. 57, no. 1, pp.107-121, January 2010.

[8] N. Bianchi, M. Dai Pré, G. Grezzani and S. Bolognani, "Design considerations on fractional-slot fault-tolerant synchronous motors" *IEEE*

[9] C. Spargo, B. Mecrow and J. Widmer, "Design of a Synchronous Reluctance Motor with Non-Overlapping Fractional-Slot Concentrated Windings" *IEEE, Transactions on*, vol., no.99, pp.

[10] J. Cros, P. Viarouge "Synthesis of High Performance PM Motors With Concentrated Windings" *IEEE, Transactions on Energy Conversion*, vol. 17, no. 2, pp.248-253, January 2002.

[11] N. Bianchi, S. Bolognani "Design optimisation of electric motors by genetic algorithms" *IEE, Proc.-Electr. Power Appl.*, vol. 145, no. 5, pp.475-483, January 1998.

[12] P. Alotto, M. Barcaro, N. Bianchi, M. Guarnieri "Optimization of Interior PM Motors With Machaon Rotor Flux Barriers" *IEEE, Transactions on Magnetics*, vol. 47, no. 5, pp.958-961, May 2011.

[13] J. Martinez, K. Krischan, A. Muetze, P. Handgruber "Design of a PM machine using multi-objective GA methods and FEM validation".

[14] P.A. Hargreaves, B.C. Mecrow, R. Hall "Calculation Of Iron Loss In Electrical Generators Using Finite Element Analysis".